Electronic Supplementary Information

Dual-functionalization actuated trimodal attribute in an ultra-robust MOF: exceptionally selective capture and effectual fixation of CO$_2$ with fast-responsive, nanomolar detection of assorted organo-contaminants in water

Nilanjan Seal,[a,b] Manpreet Singh,[a,b] Sandeep Das,[c] Ranadip Goswami,[a,b] Biswarup Pathak,[c] and Subhadip Neogi*[,a,b]

[a]Academy of Scientific and Innovative Research (AcSIR), Ghaziabad- 201002, India

[b]Inorganic Materials & Catalysis Division, CSIR-Central Salt & Marine Chemicals Research Institute, Bhavnagar, Gujarat 364002, India

[c]Discipline of Chemistry, Indian Institute of Technology (IIT) Indore, Indore, Madhya Pradesh 453552, India

*E-mail: sneogi@csmcri.res.in

Table of contents

cycles of CO₂ cycloaddition reaction.

Materials and Physical measurements

All the solvents andreagents were purchased from commercial sources(except H_3TCA) and used without furtherpurification.Thermogravimetric analyses (TGA) (heating rate of 10 °C/min under N_2 atmosphere) were performed with a Mettler Toledo Star SW 8.10 system.The Fourier Transform infrared-spectra (IR) of the samples were recorded using the KBr pellet method on a Perkin–Elmer GX FTIR spectrometer in the region of 400–4000 cm^{-1}. Powder X-ray diffraction (PXRD) data were collected using a PANalytical Empyrean (PIXcel 3D detector) system equipped with Cu Kα (λ=1.54 Å) radiation.Microanalyses of the compounds were conducted using elementarvario MICRO CUBE analyzer. UV-Vis spectra recorded using Shimadzu UV-3101 PC spectrometer and the luminescence experiments were performed at

room temperature using a Fluorolog Horiba Jobin Yvon spectrophotometer. Surface area measurement was carried out using Micromeritics ASAP 2020 analyser.

Single Crystal X-ray Crystallography

Single crystals with suitable dimensions were chosen under an optical microscope and mounted on a glass fibre for data collection. Intensity data for as synthesized colorless crystal of **CSMCRI-9** were collected using graphite-monochromatedMoK$_\alpha$ (λ=0.71073 Å) radiation on a Bruker SMART APEX diffractometer equipped with CCD area detector at 173 K, The linear absorption coefficients, scattering factors for the atoms, and the anomalous dispersion corrections were taken from International Tables for X-ray Crystallography. The data integration and reduction were performed with SAINT[1] software. Absorption corrections to the collected reflections were accounted with SADABS[2] using XPREP.[3] The structure was solved by direct method using SIR-97[4] and was refined on F2 by the full-matrix least-squares technique using the SHELXL-2014[5] program package. All H atoms were placed in calculated positions using idealized geometries (riding model) and assigned fixed isotropic displacement parameters using the SHELXL default. To give an account of disordered electron densities associated with solvent molecules, the "SQUEEZE" protocol in PLATON[6] was applied that produced a set of solvent free diffraction intensities. Final cycles of least-squares refinements improved both the R values and Goodness of Fit with the modified data set after subtracting the contribution from the disordered solvent molecules, using SQUEEZE program. The crystal and refinement data for solvent free **CSMCRI-9** is listed in Table S1. Topological analysis was performed by using TOPOS software.[7]

Experimental section

Synthesis of CSMCRI-9. A mixture of Cd(NO$_3$)$_2$·4H$_2$O (30 mg, 0.1 mmol), bpg (21.6 mg, 0.05 mmol) and H$_3$TCA (19 mg, 0.05 mmol) was dissolved in 4 mL of N,N-Dimethylacetamide (DMA) and 2 mL of distilled water in a 15 mL screw-capped vial by ultrasonic treatment for 15 min. Then it was heated to 85 °C for 4 days, and then slowly cooled down to room temperature. The colorless, shiny and block shaped X-ray quality crystals were obtained; which were then filtered, thoroughly washed with DMA and air dried (yield: 65 %). Anal. Calcd. For [Cd$_{1.5}$(TCA)(bpg)$_{0.5}$(H$_2$O)]·3DMA·2H$_2$O: C, 45.76; H, 5.12; N, 6.84. Found: C, 44.97; H, 4.93; N, 6.90

CO$_2$ Cycloaddition Reaction. In a 10 mL teflon-lined stainless steel autoclave, 21.91 mmol of epoxide, 0.35 mol % of activated catalyst and 0.36 mol % of Bu$_4$N$^+$Br$^-$ were purged with 1.0 MPa of CO$_2$. The mixture was heated to 65 °C for 6 h at 600 rpm. After that, the reactor was cooled down and the product was centrifuged to separate the catalyst and analysed by GC and ^{1}H-NMR. The recovered catalyst was thoroughly washed with acetone followed by air drying and reused for next cycle of experiment.

Fluorescence Measurements. In a typical procedure, 1 mg of finely ground **9a** was dispersed in 2 mL of water to form a stable suspension after ultrasonic treatment for two hours. All fluorescence titration experiments were performed by gradually adding aqueous solution of

nitroanalytes (1 mM) and antibiotics (1 mM) {DMF-water mixed solution for pesticides (1 mM)}. Fluorescence detections were performed at the emission wavelength ranging from 370 to 650 nm with an excitation wavelength (λ_{ex}) of 338 nm and a slit width of 4 nm at room temperature. During the whole period of performing each titration, the dispersion was continuously stirred to maintain the uniformity. All titrations were conducted thrice, and consistent results were reported.

Recyclable luminescence experiments. The reproducibility of **9a** towards sensing of DCNA, TNP and NZF was studied. After the first sensing experiment, the MOF powder was recovered by centrifugation and washed thoroughly with water and air dried. Subsequently, this recovered material was used for the next cycle of experiments.

Synthesis of the Ligand

The ligand 4,4',4''-tricarboxytriphenylamine (H$_3$TCA) was prepared by following a literature method[8]and characterized by NMR and ESI-MS analysis.
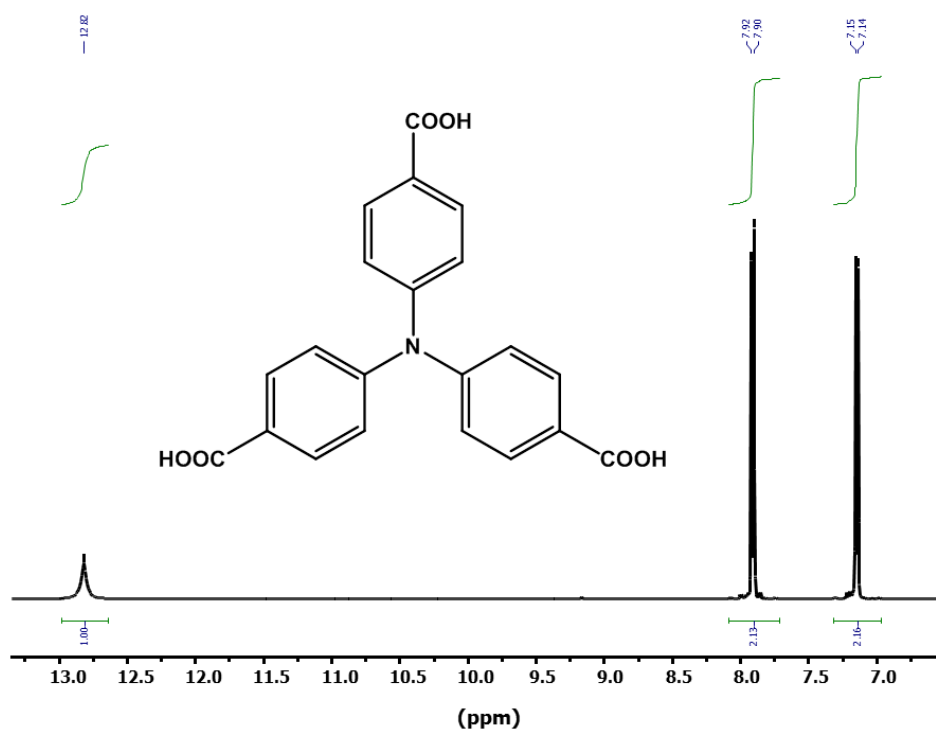
Fig. S1.^{1}H-NMR spectrum of 4,4',4''-tricarboxytriphenylamine (H$_3$TCA).
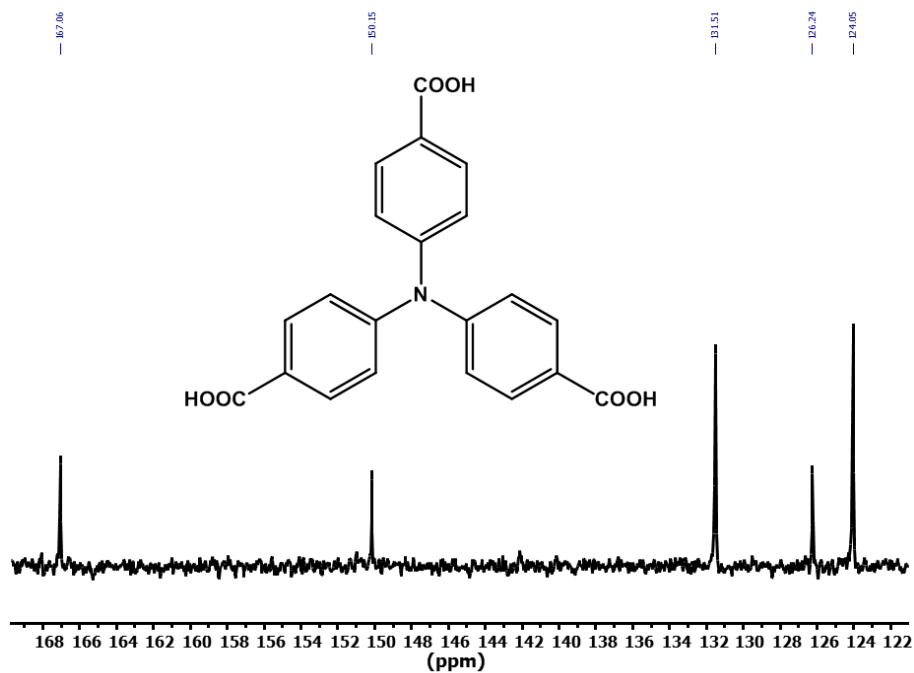
Fig. S2. ^{13}C-NMR spectrum of 4,4',4''-tricarboxytriphenylamine (H$_3$TCA).
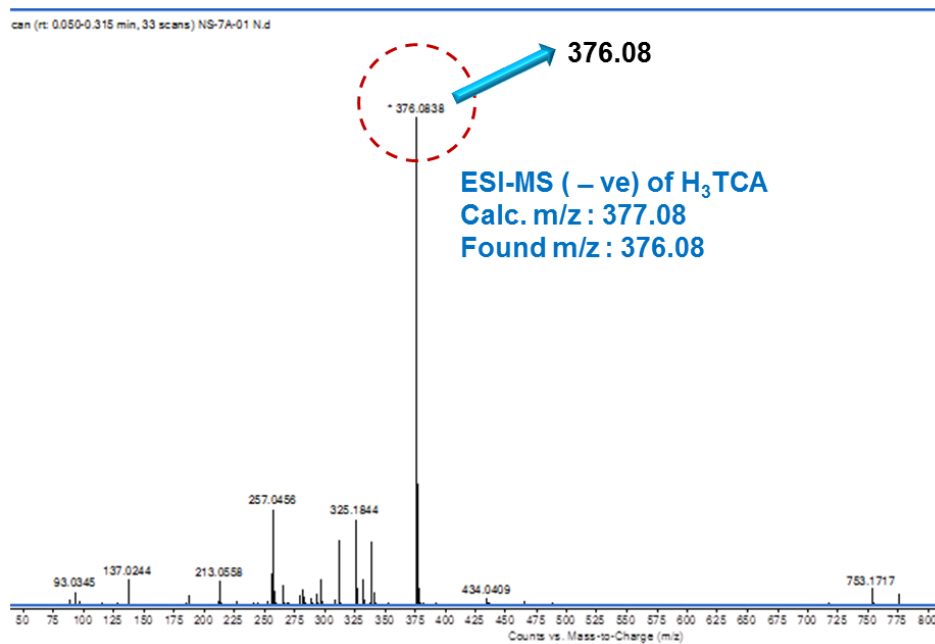
Fig. S3. ESI-MS spectrum of 4,4',4''-tricarboxytriphenylamine (H$_3$TCA).
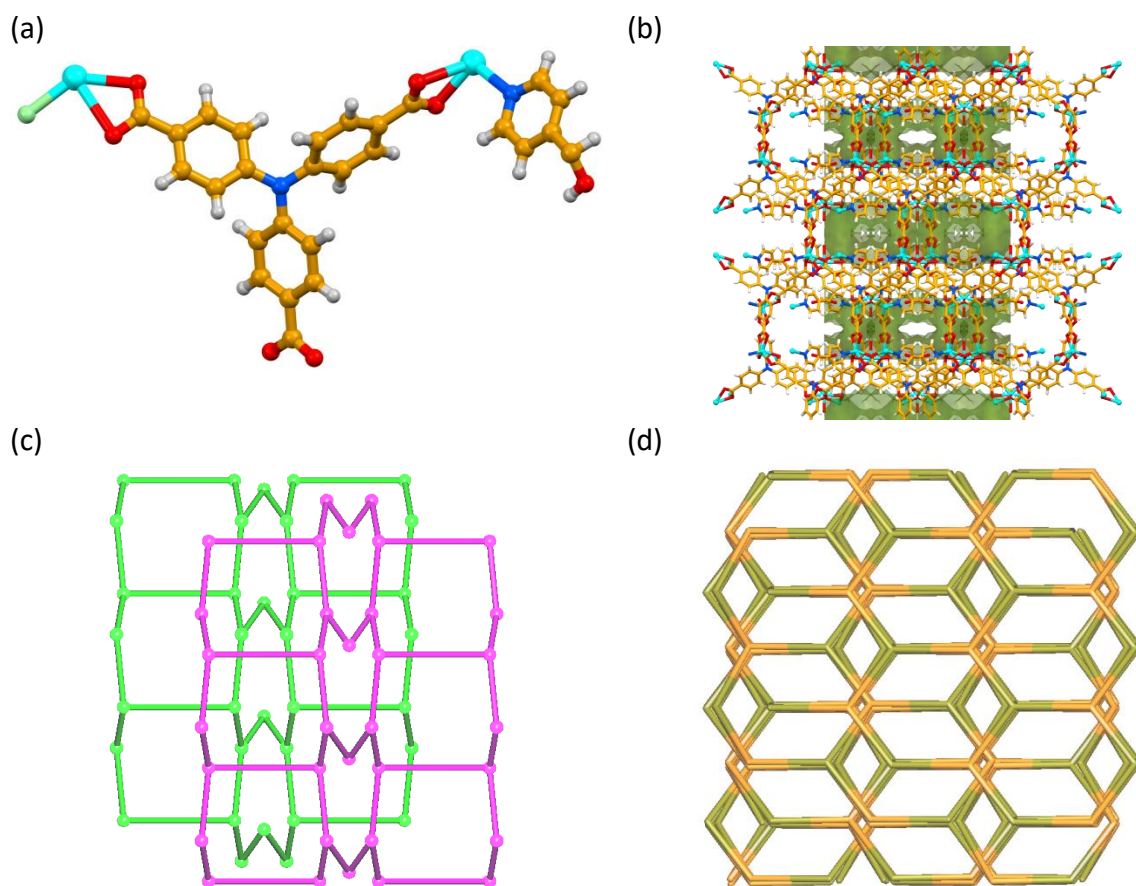
Fig. S4. (a) Asymmetric unit of **CSMCRI-9**. (b) Void view of **CSMCRI-9** along crystallographic *c*-axis. (c) and (d) Topological representation of **CSMCRI-9**.
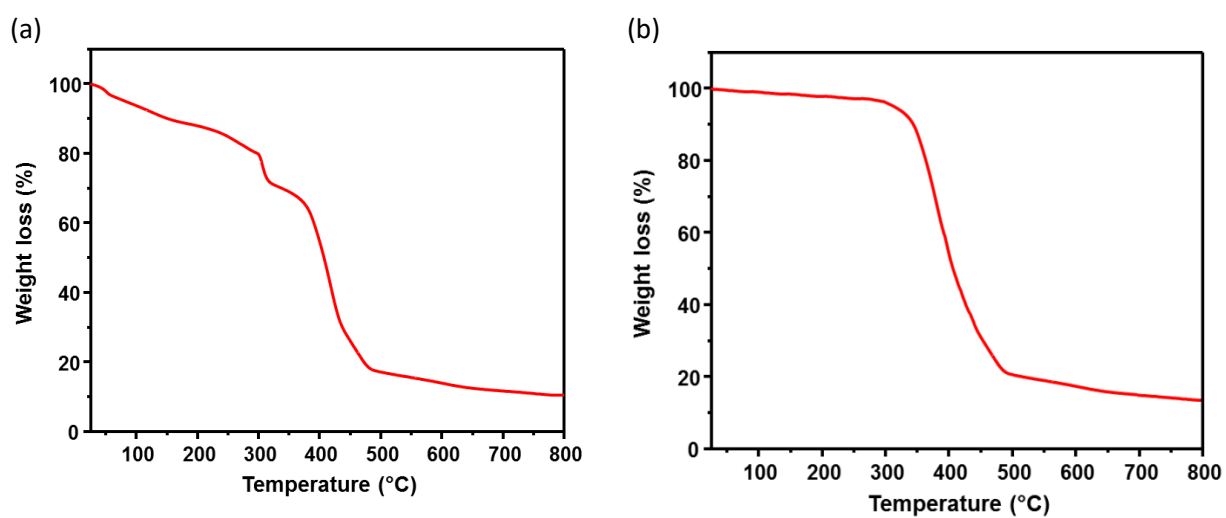
Fig. S5.Thermogravimetric analysis of (a) **CSMCRI-9** and (b) **9a**.
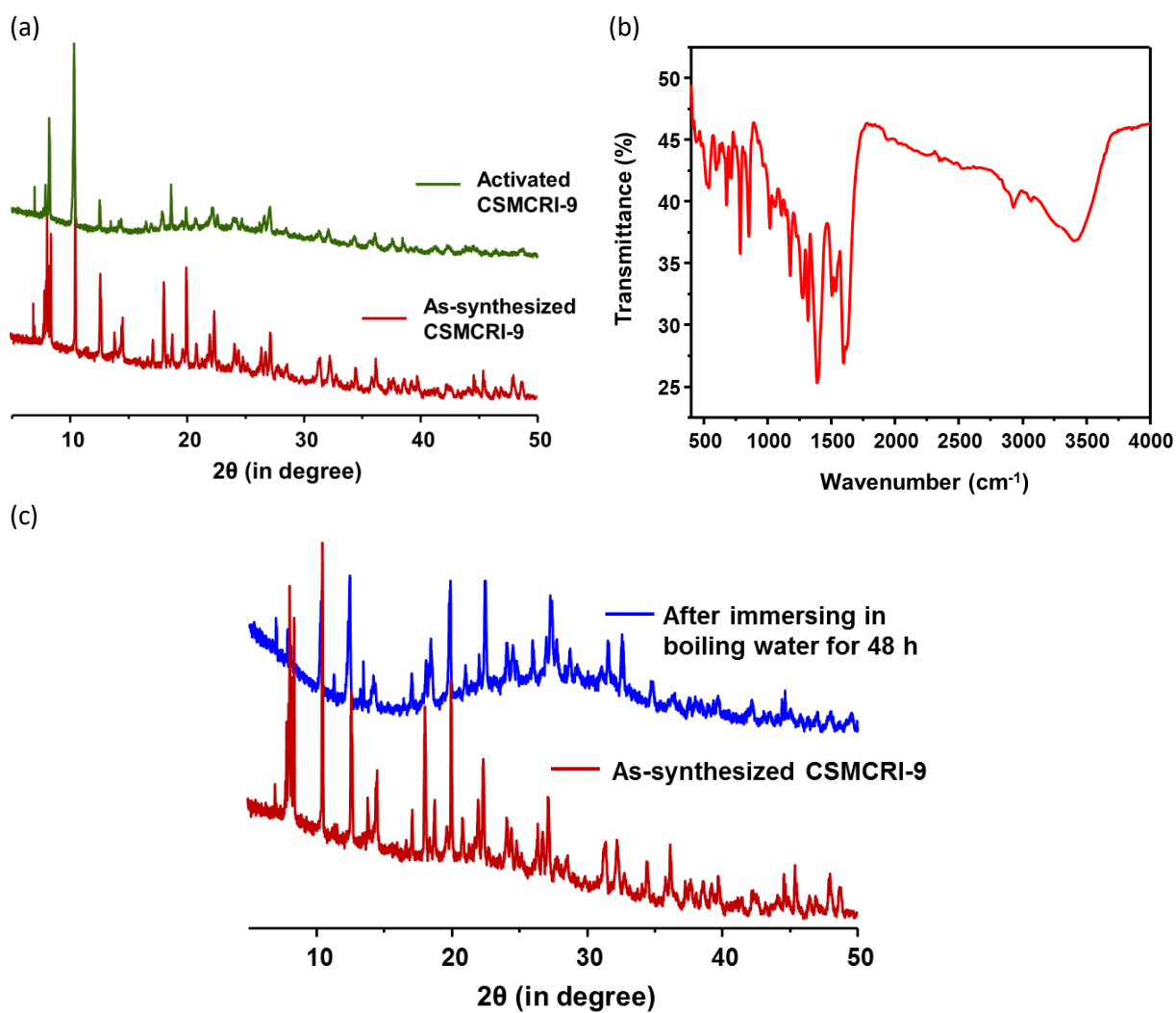
Fig. S6. (a) As-synthesized (red) and activated (green) PXRD pattern of **CSMCRI-9**. (b) FT-IR spectra (KBr pellets, cm^{-1}) of **CSMCRI-9**. (c) PXRD pattern of **CSMCRI-9** in boiling water showing structural stability up to 48 hours.
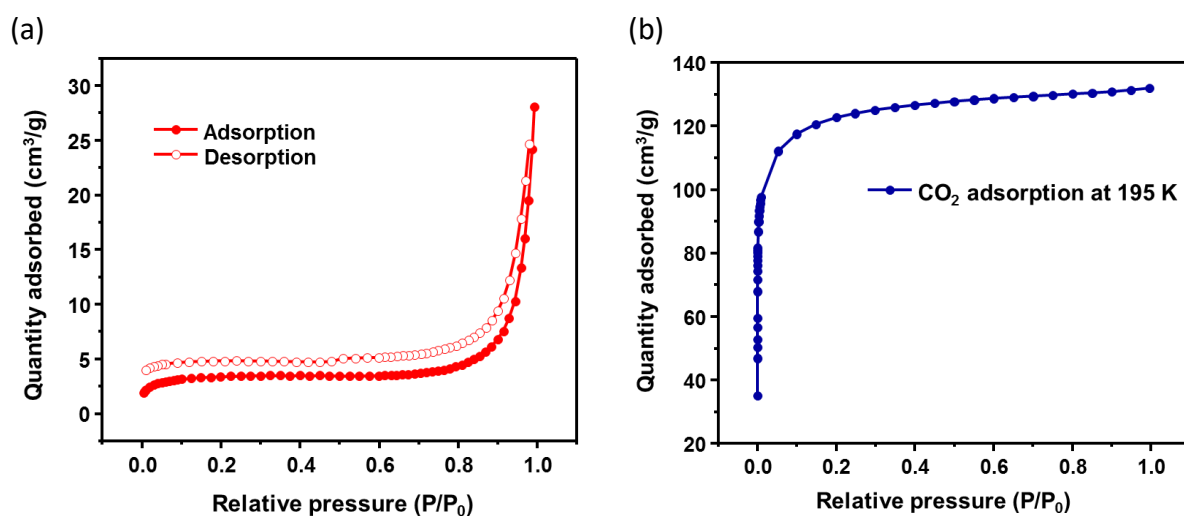
Fig. S7. (a) N_2 adsorption isotherm of activated **CSMCRI-9** at 77 K. (b) CO_2 adsorption isotherm of activated **CSMCRI-9** at 195 K.

Calculations of Adsorption Selectivity by IAST method

Ideal Adsorption Solution Theory (IAST) was used to predict mixed-gas adsorption equilibria from single component isotherms. The Langmuir equation as given below was successful for fitting our data, where, q is the adsorbed amount per mass of adsorbent, q_m is the saturation capacity, b is the affinity coefficient of adsorption sites, and p is the pressure of the bulk gas at equilibrium with the adsorbed phase. The fitted parameters were then used to predict single-component adsorption with IAST.

$$q = \frac{q_m \, bp}{1 + bp}$$

Based on the above equation parameters of pure gas adsorption, we used IAST model to investigate the separation of gas mixtures CO_2/N_2 and CO_2/CH_4 with 15/85 composition. The inputs to the IAST calculations are pure-component adsorption isotherms at the temperature of interest, and the output is the adsorption selectivity is defined by the following equation,

$$S_{ads} = \frac{q_{CO2} / q_{other}}{p_{CO2} / p_{other}}$$

Where, q_{CO2} and q_{other} are the absolute component loadings of the adsorbed phase in the mixture and p_{CO2} and p_{other} are the corresponding relative pressure.
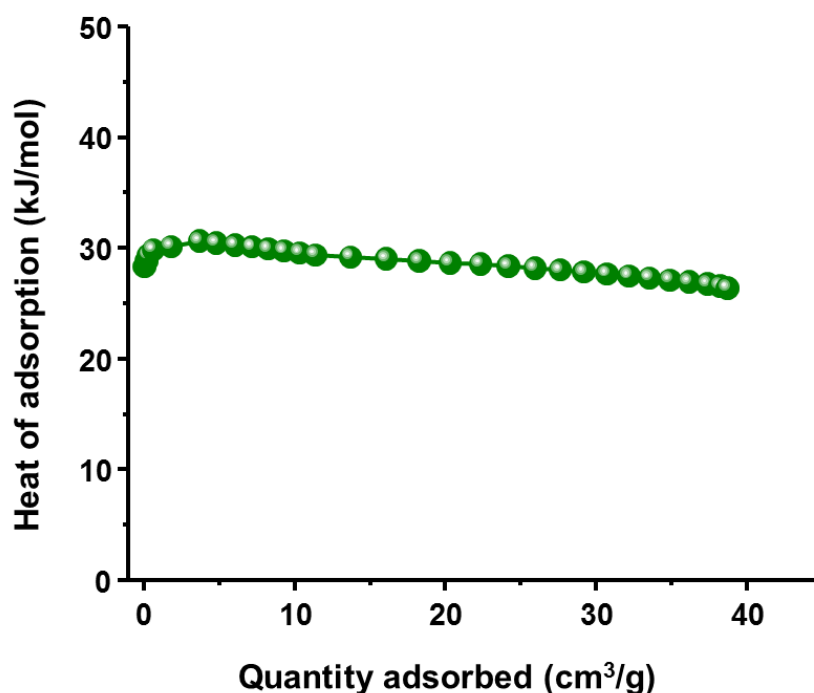
Fig. S8. The isosteric heat of adsorption (Q_{st}) curve for **9a**.
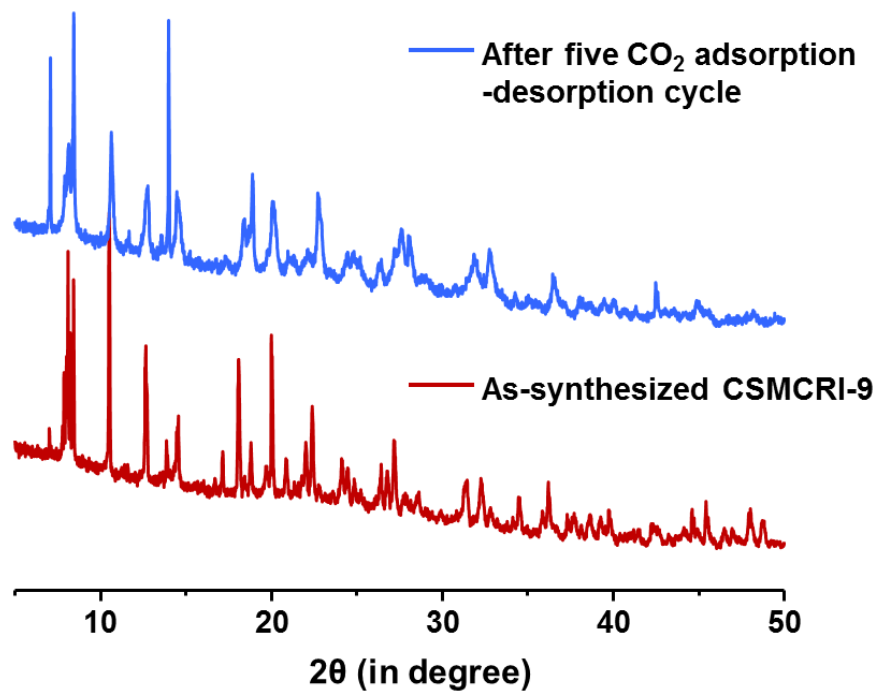
Fig. S9. PXRD patterns of **9a** obtained after five CO₂ adsorption-desorption cycles, revealing that structural integrity of the framework is maintained.
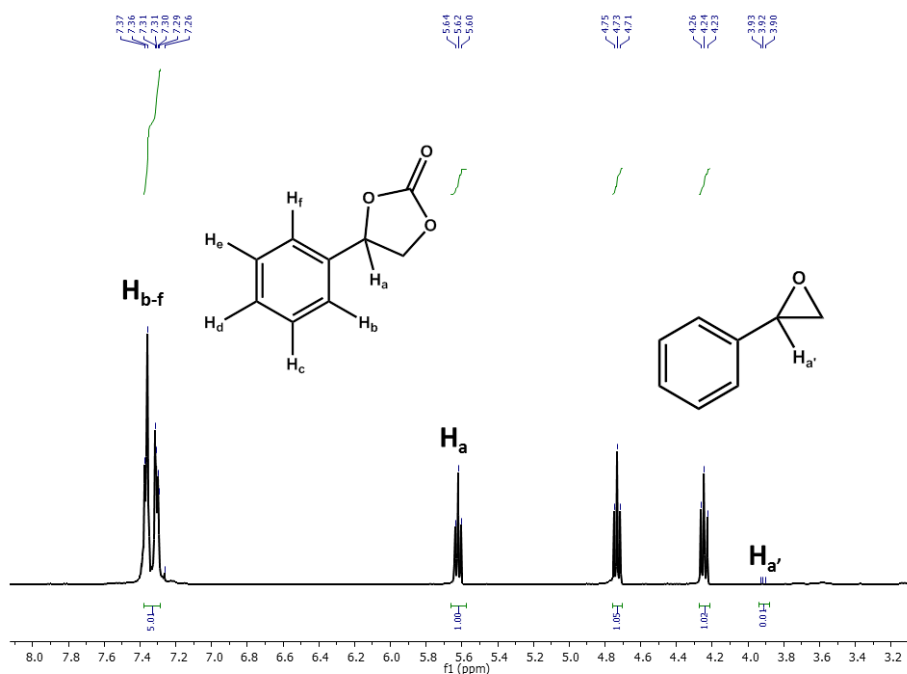
Fig. S10. ¹H-NMR spectra of styrene carbonate (4-Phenyl-1,3-dioxolan-2-one). The peak at 7.26 is for CDCl₃.
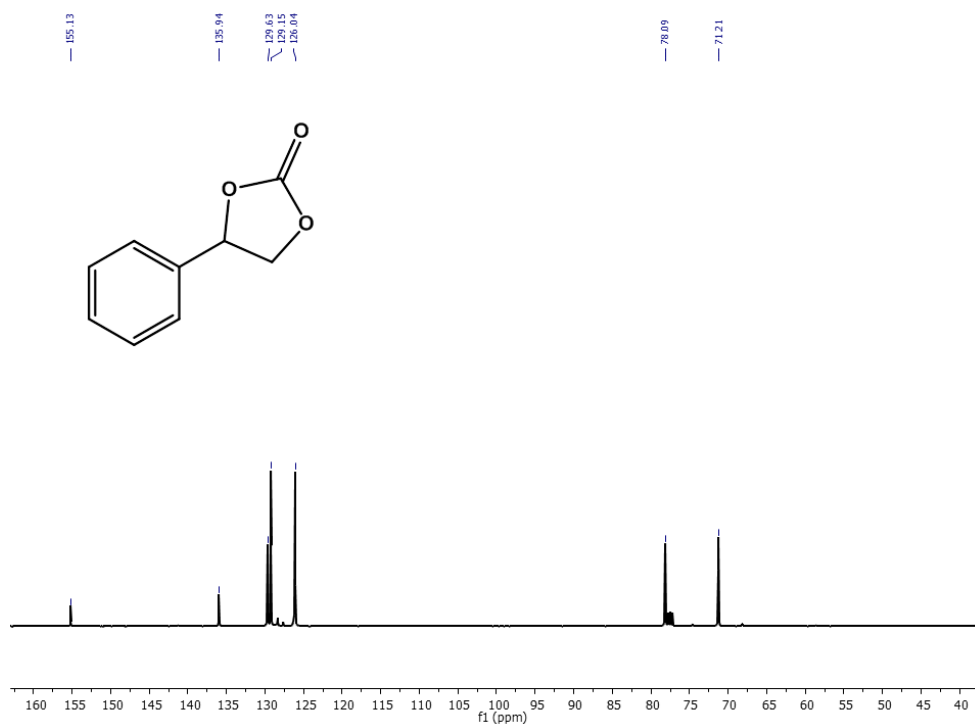
Fig. S11. ^{13}C-NMR spectra of styrene carbonate (4-Phenyl-1,3-dioxolan-2-one).
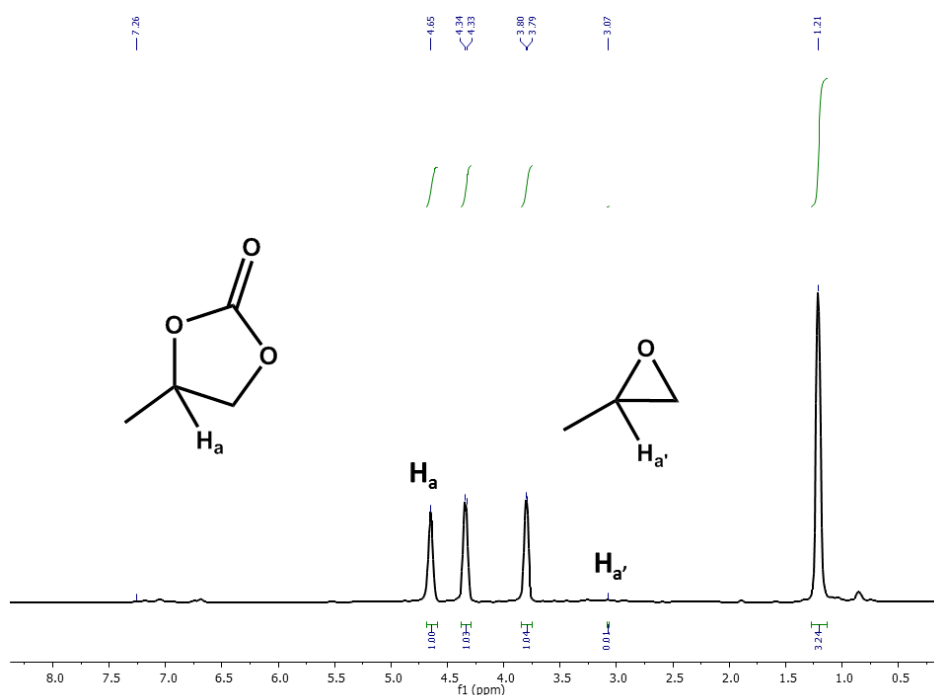
Fig. S12. ^{1}H-NMR spectra of propylene carbonate (4-Methyl-1,3-dioxolan-2-one). The peak at 7.26 is for CDCl$_3$.

Fig. S13. ^{13}C-NMR spectra of propylene carbonate (4-Methyl-1,3-dioxolan-2-one).

Fig. S14. ^{1}H-NMR spectra of butylene carbonate (4-Ethyl-1,3-dioxolan-2-one). The peak at 7.26 is for CDCl$_3$.
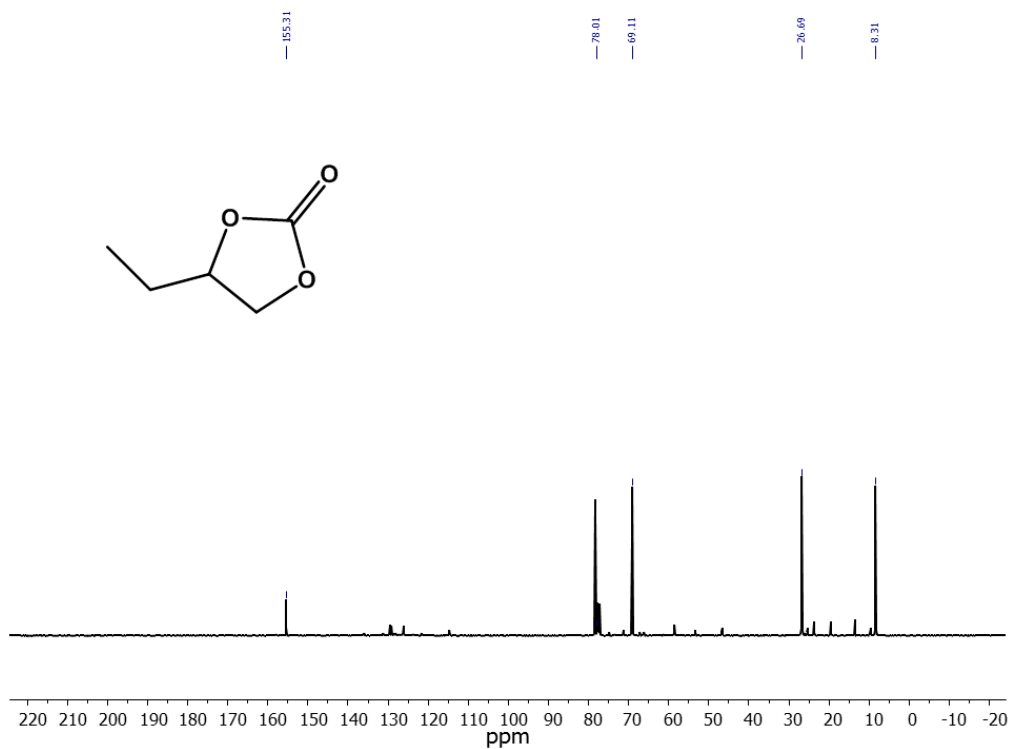
Fig. S15. ^{13}C-NMR spectra of butylene carbonate (4-Ethyl-1,3-dioxolan-2-one).
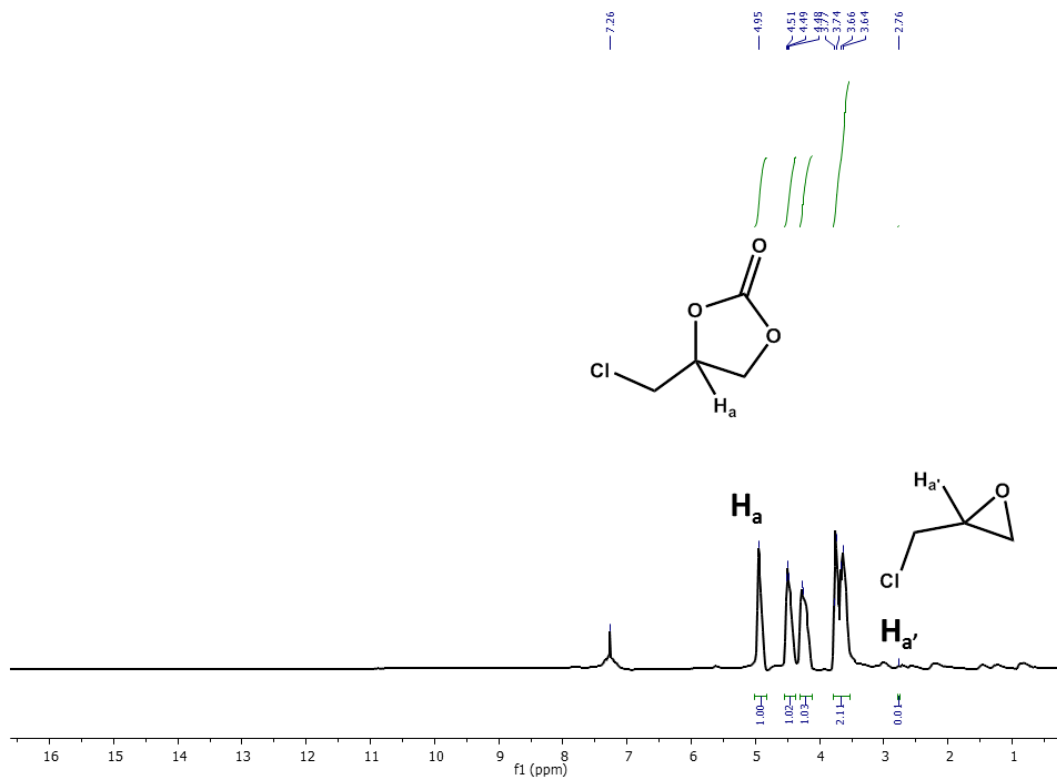
Fig. S16. ^{1}H-NMR spectra of epichlorohydrin carbonate (4-(chloromethyl)-1,3-dioxolan-2-one). The peak at 7.26 is for CDCl$_3$.
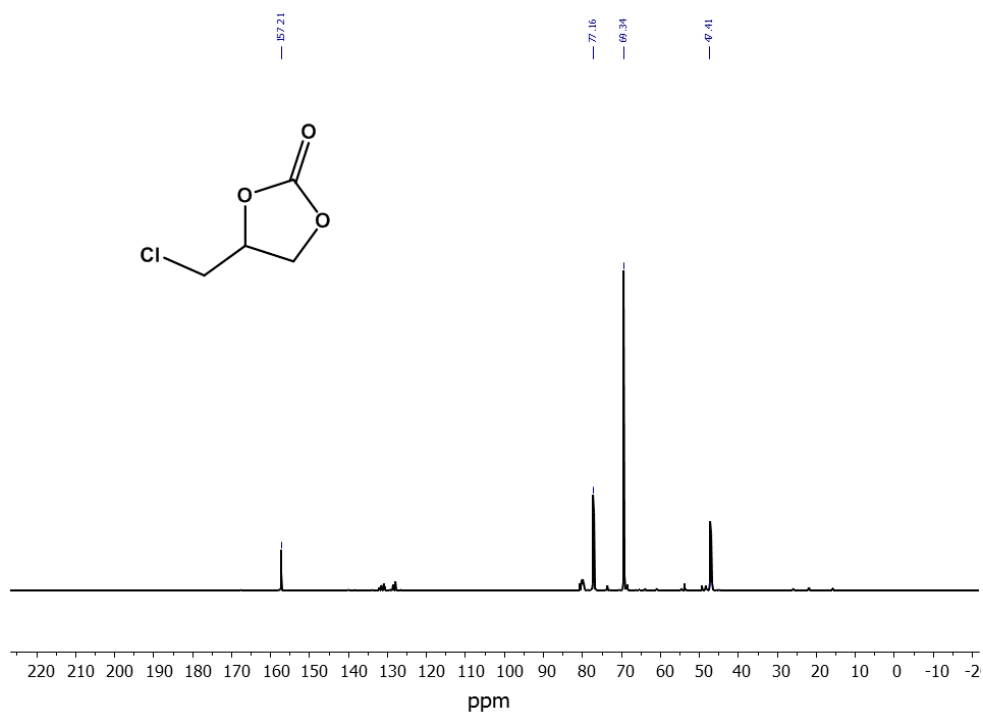
Fig. S17. ^{13}C-NMR spectra of epichlorohydrin carbonate (4-(chloromethyl)-1,3-dioxolan-2-one).
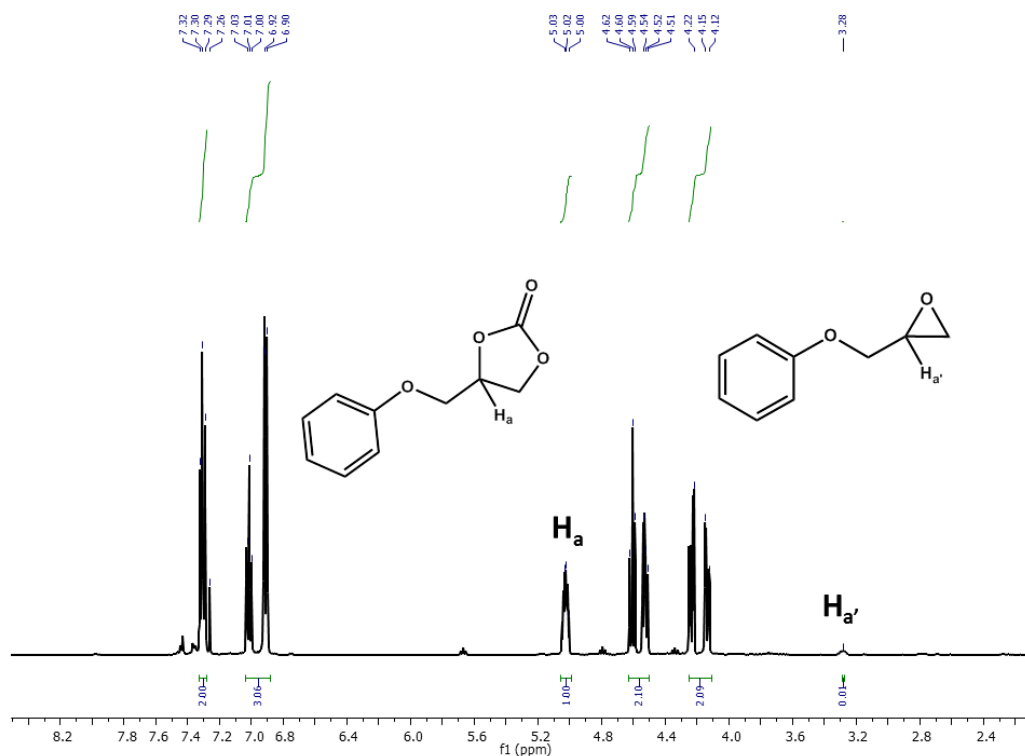
Fig. S18. ^{1}H-NMR spectra of phenyl glycidyl carbonate (4-(phenoxymethyl)-1,3-dioxolan-2-one). The peak at 7.26 is for CDCl$_3$.
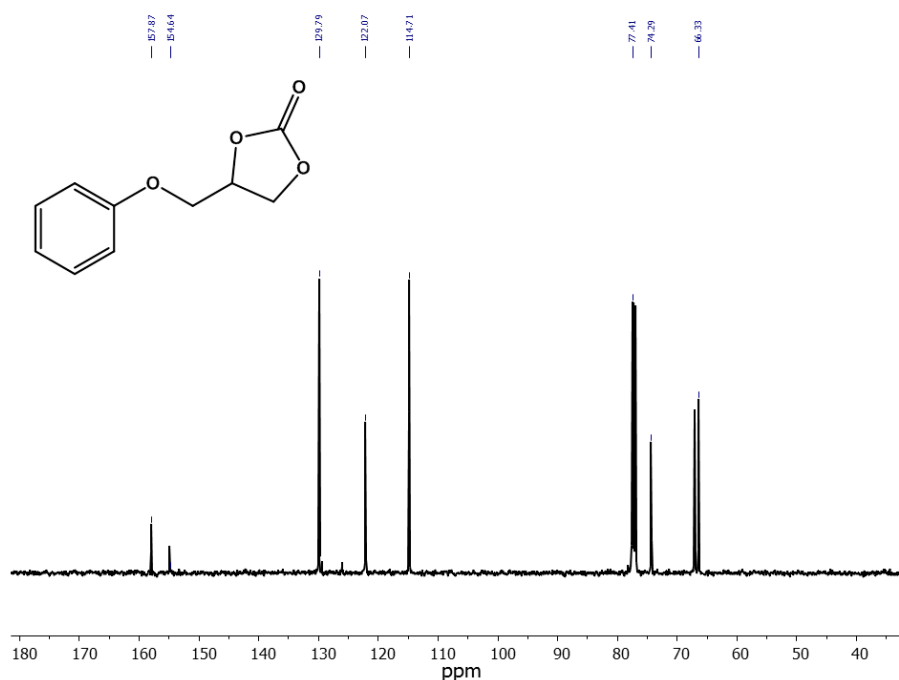
Fig. S19. ^{13}C-NMR spectra of phenyl glycidyl carbonate (4-(phenoxymethyl)-1,3-dioxolan-2-one).

Calculation details of conversion, yield and selectivity for the CO_2 cycloaddition reaction catalyzed by activated CSMCRI-9:

The conversion, yield and selectivity for CO_2 cycloaddition reaction, catalyzed by activated **CSMCRI-9** (**9a**) were calculated from the integral area of the characteristic protons of styrene carbonate, styrene oxide and phenyl ring. From literature reference,[9] the characteristic protons for styrene carbonate and styrene oxide were identified.

The formula are

Conversion (%) = [1-{$5I_{Ha'}/I_{H(b-f)}$}]×100 %

Yield (%) = {$5I_{Ha}/I_{H(b-f)}$}×100 %

Selectivity (%) = [$5I_{Ha}/${ $I_{H(b-f)}-5I_{Ha'}$}]×100 %

where, I_{Ha} is the integral area of the characteristic proton of styrene carbonate; $I_{Ha'}$ is the integral area of the characteristic proton of styrene oxide and $I_{H(b-f)}$ is the integral area of the protons of phenyl ring.

From Fig. S10, for styrene carbonate, I_{Ha}= 1.00, $I_{Ha'}$ = 0.01 and $I_{H(b-f)}$ = 5.01

Therefore, conversion (%) = {1-(5×0.01/5.01)}×100 % = 99 %

Yield (%) = (5×1/5.01) ×100 % = 99.8 %

Selectivity (%) = [(5×1)/{5.01-(5×0.01)}] ×100 % = 100 %

For the other four compounds, the conversion, yield and selectivity were determined by the following formula

Conversion (%) = {I_{Ha}/ (I_{Ha}+$I_{Ha'}$)} ×100 %

Yield (%) = {I_{Ha}/ (I_{Ha}+$I_{Ha'}$)} ×100 %

Selectivity (%) = (Yield of the desired product/total yield of the products) ×100 %

From Fig. S16, for epichlorohydrine carbonate, I_{Ha}= 1.00, $I_{Ha'}$ = 0.01

Therefore, conversion for epichlorohydrine carbonate = {1/(1+.01)} ×100 % = 99 %

yield of epichlorohydrine carbonate = {1/(1+.01)} ×100 % = 99 %

selectivity = {0.99/(0.99+0.01)}×100 % = 99 %
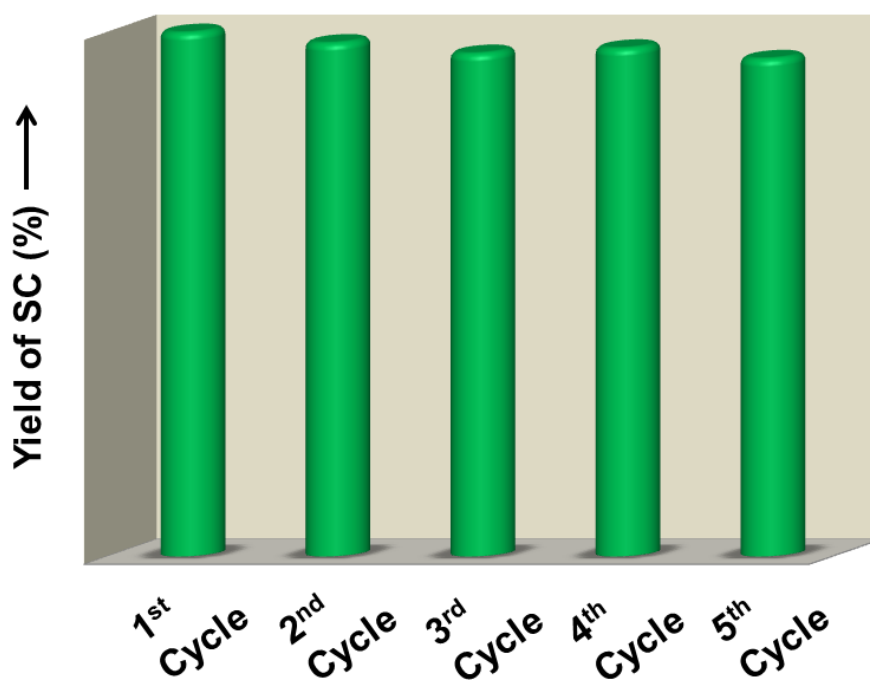
Fig. S20. Recyclability test of the catalyst up to five runs, showing negligible loss in catalytic activity.
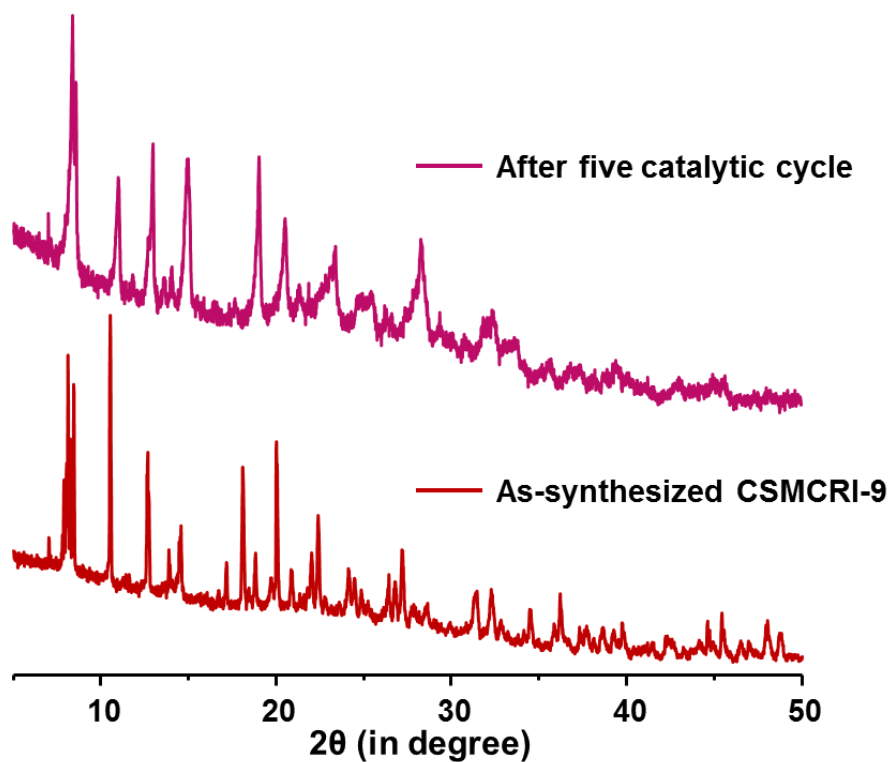
Fig. S21. PXRD patterns of **9a** obtained after five consecutive catalytic cycles of CO_2 cycloaddition reaction, revealing that structural integrity of the framework is maintained.
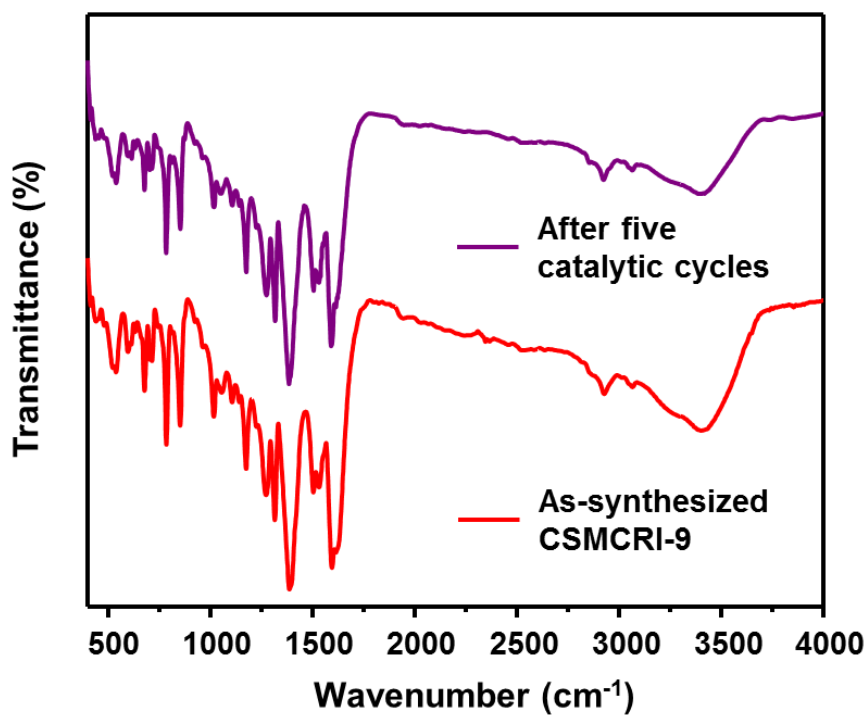
Fig. S22. FT-IR spectra of **9a** obtained after five consecutive catalytic cycles of CO_2 cycloaddition reaction.
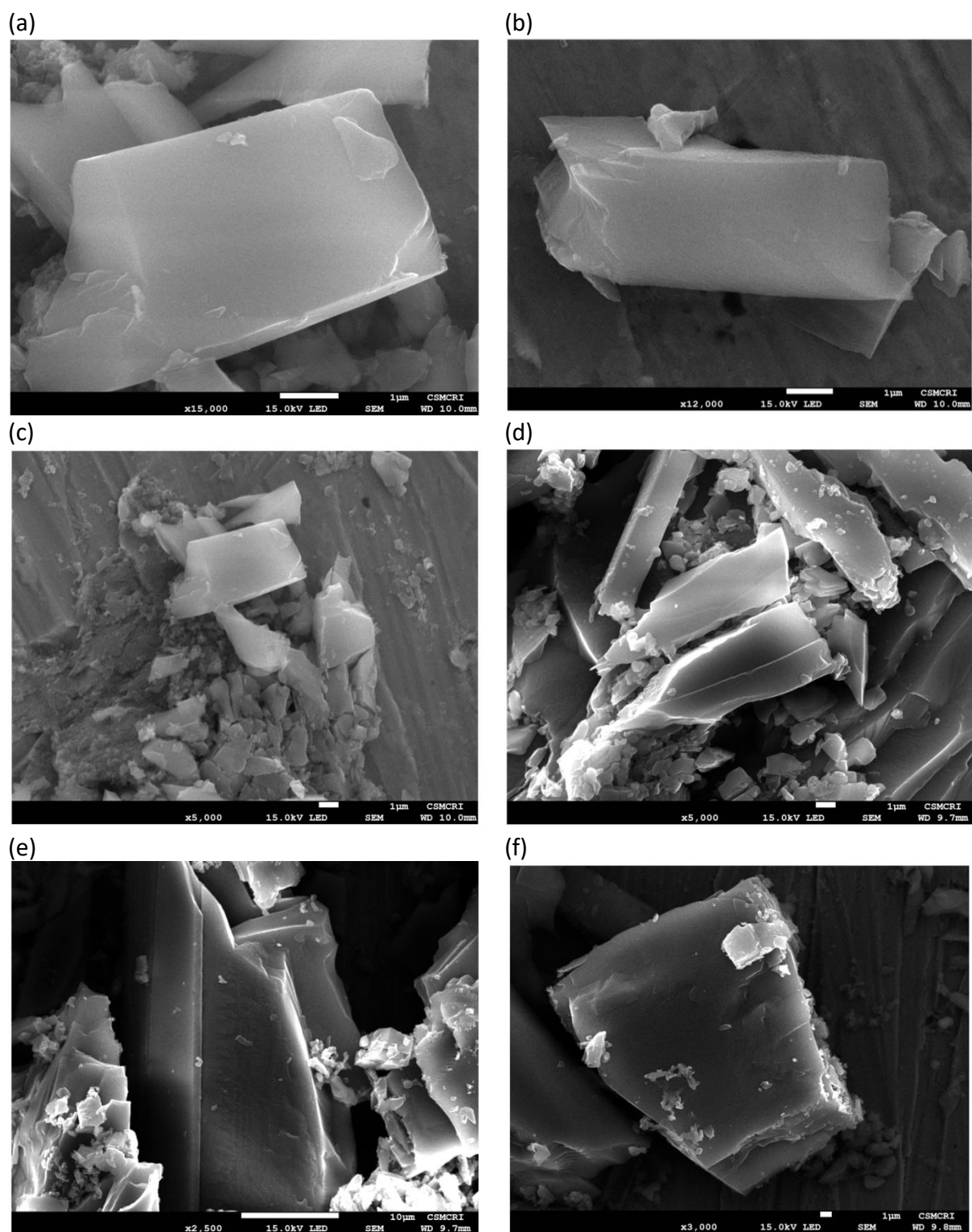
Fig. S23. a), b) and c) FE-SEM images of **CSMCRI-9**. d), e) and f) Images of **9a** obtained after five consecutive catalyst recyclability studies showing rectangular block shaped morphology is maintained.
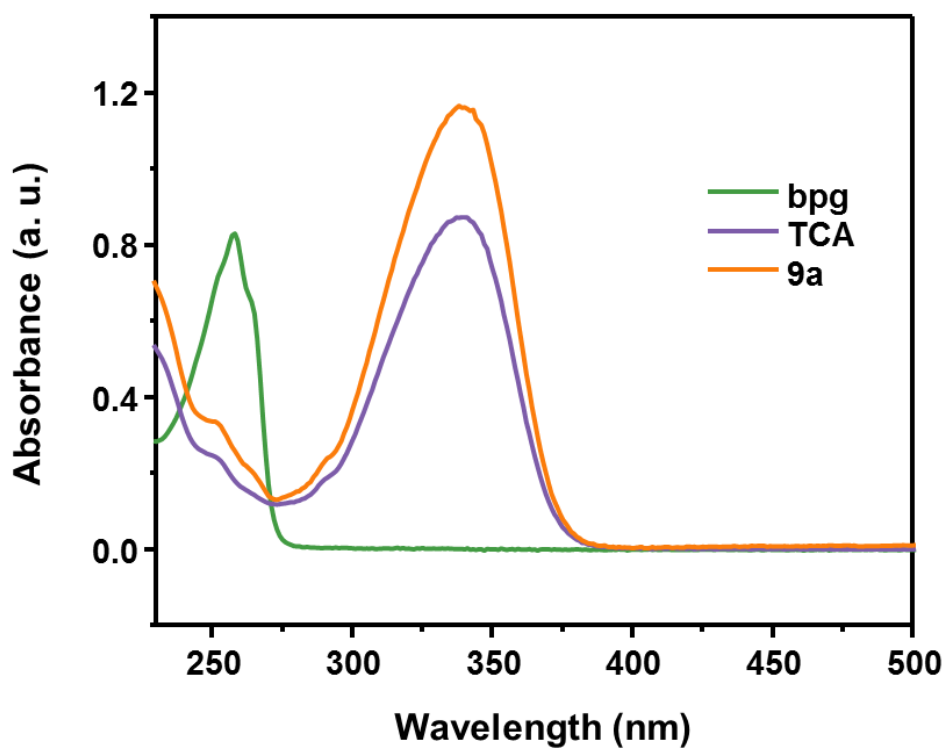
Fig. S24. UV-Vis spectra of H_3TCA, bpg and **9a** (dispersed in water).
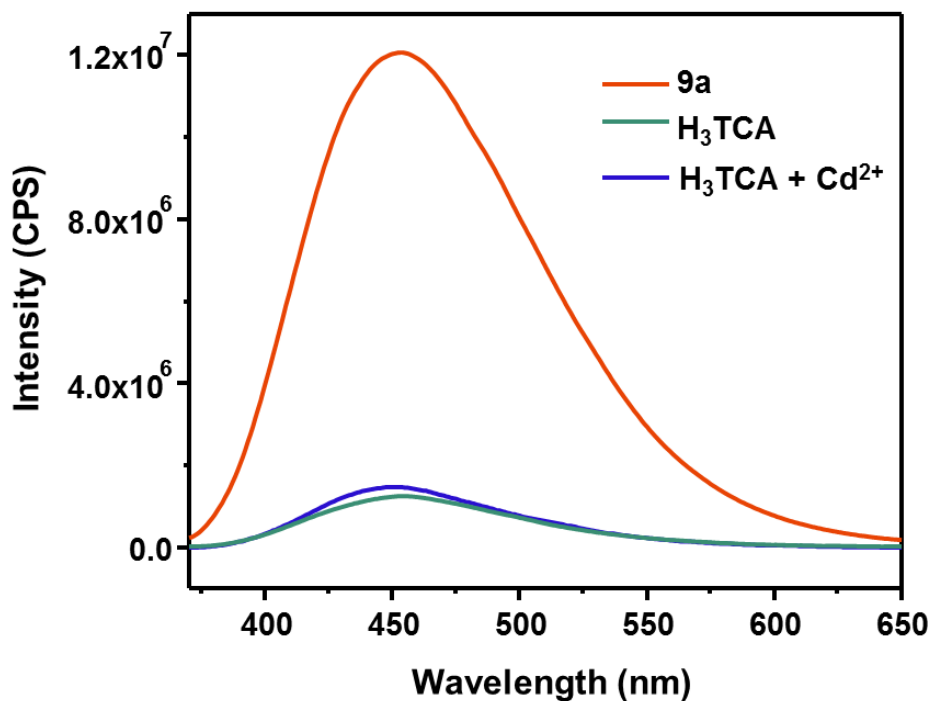
Fig. S25. Emission intensity of H_3TCA, **9a** and a mixture of H_3TCA with Cd^{2+} (dispersed in water).
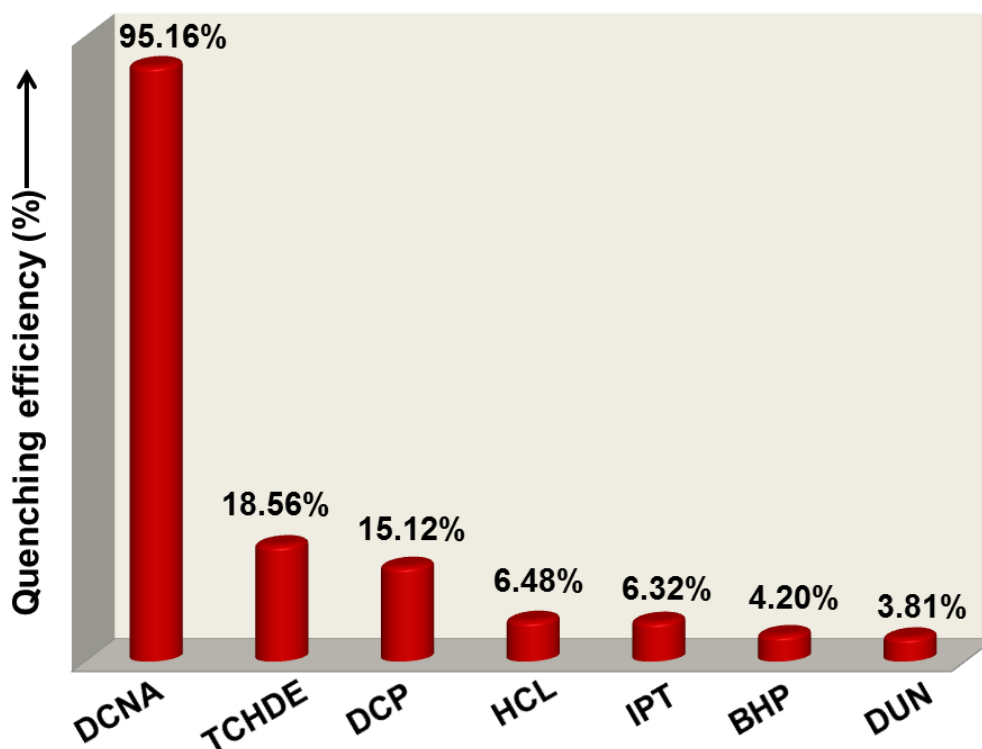
Fig. S26. Fluorescence quenching efficiency of **9a** (1 mg/ 2 mL water) for studied pesticides. Quenching efficiency of **9a** is calculated using equation $(I_0 − I)/I_0 × 100\%$, where I_0 and I denotes the emission intensities before and after the addition of studied pesticides, respectively.

Fig. S27. Emission spectra of **9a** upon incremental addition of 2,4,4'-Trichloro-2'-hydroxydiphenyl Ether (TCHDE) solution (1 mM, 200 μL).

Fig. S28. Emission spectra of **9a** upon incremental addition of 2,4-Dichlorophenol (DCP) solution (1 mM, 200 µL).

Fig. S29. Emission spectra of **9a** upon incremental addition of hexaconazole (HCL) solution (1 mM, 200 µL).

Fig. S30. Emission spectra of **9a** upon incremental addition of isoproturon (IPT) solution (1 mM, 200 µL).

Fig. S31. Emission spectra of **9a** upon incremental addition of 2,2-Bis(4-hydroxyphenyl) propane (BHP) solution (1 mM, 200 µL).
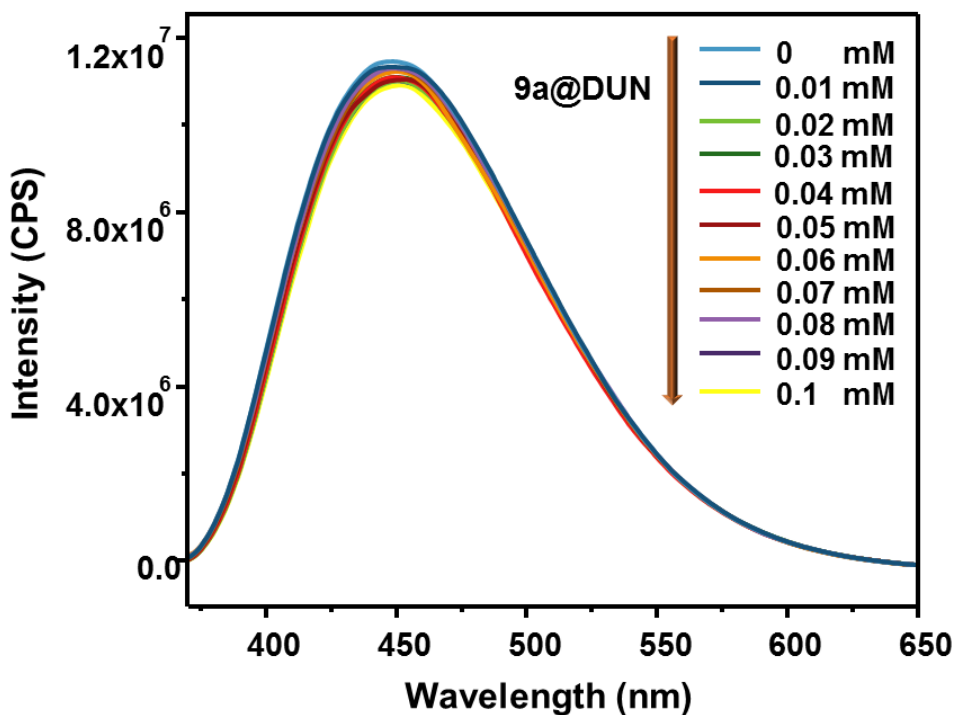
Fig. S32. Emission spectra of **9a** upon incremental addition of diuron (DUN) solution (1 mM, 200 μL).

Fig. S33. The curvature of the S–V plot for 1 mM DCNA solution (0 to 200 μL).

Equation	y = a + b*x
Plot	B
Weight	No Weighting
Intercept	-0.07098 ± 0.0782
Slope	49.5948 ± 4.1817
Residual Sum of Squar	0.01749
Pearson's r	0.99297
R-Square (COD)	0.98598
Adj. R-Square	0.97897

Fig. S34. Stern-Volmer (S-V) plot for 1 mM DCNA solution (0 to 200 μL). The relative fluorescence intensity (I_0/I)-1 is linear with DCNA concentration in the range of 0–0.03 mM.

Equation	y = a + b*x
Plot	B
Weight	No Weighting
Intercept	1.48345E7 ± 72281.189
Slope	-1.8585E6 ± 122177.51
Residual Sum of Squ	1.47781E11
Pearson's r	-0.9811
R-Square(COD)	0.96256
Adj. R-Square	0.9684

Fig. S35. Linear region of fluorescence intensity of **9a** upon addition of DCNA (0 – 200 μL, 10 μM stock solution).

Fig. S36. Reproducibility of quenching efficiency of **9a** towards 1 mM DCNA solution up to five sensing-recovery cycles.

Fig. S37. PXRD patterns of **9a** obtained after five sensing-recovery cycles for DCNA (1 mM), revealing that structural integrity of the framework is maintained.
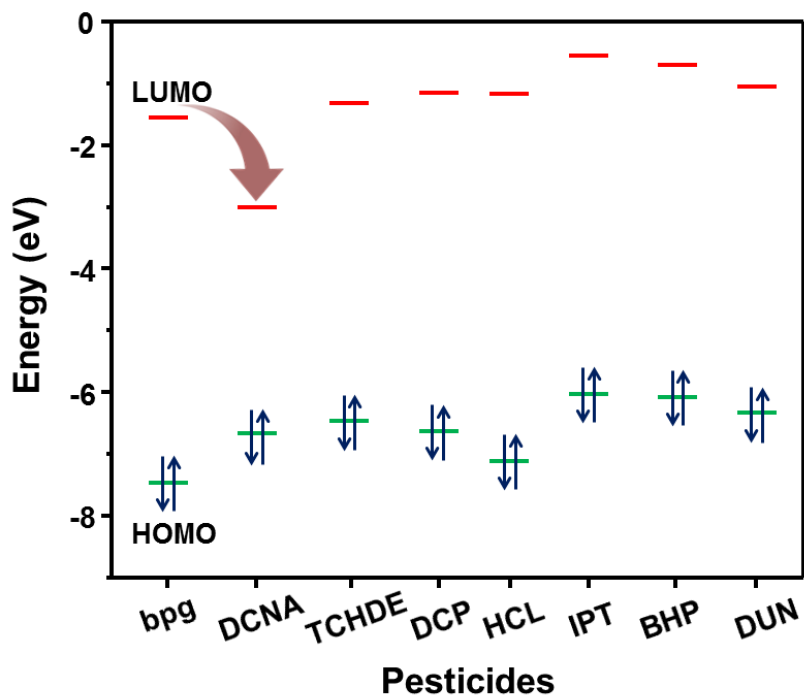
Fig. S38. HOMO–LUMO energies for bpg linker along with the studied pesticide molecules.
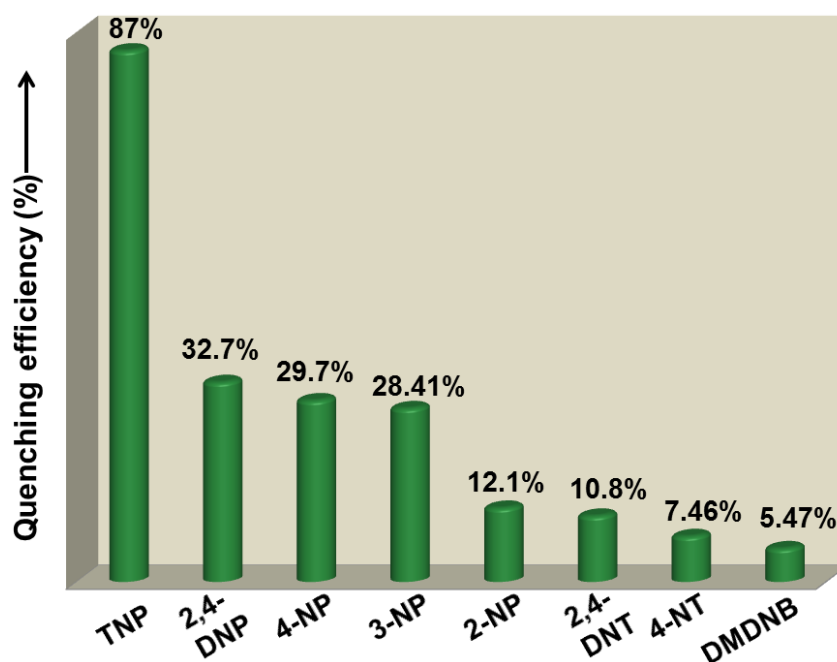
Fig. S39. Fluorescence quenching efficiency of **9a** (1 mg/ 2 mL water) towards studied nitroaromatics. Quenching efficiency of **9a** is calculated using equation $(I_0 - I)/I_0 \times 100\%$, where I_0 and I denotes the emission intensities before and after the addition of studied nitro-analytes, respectively.
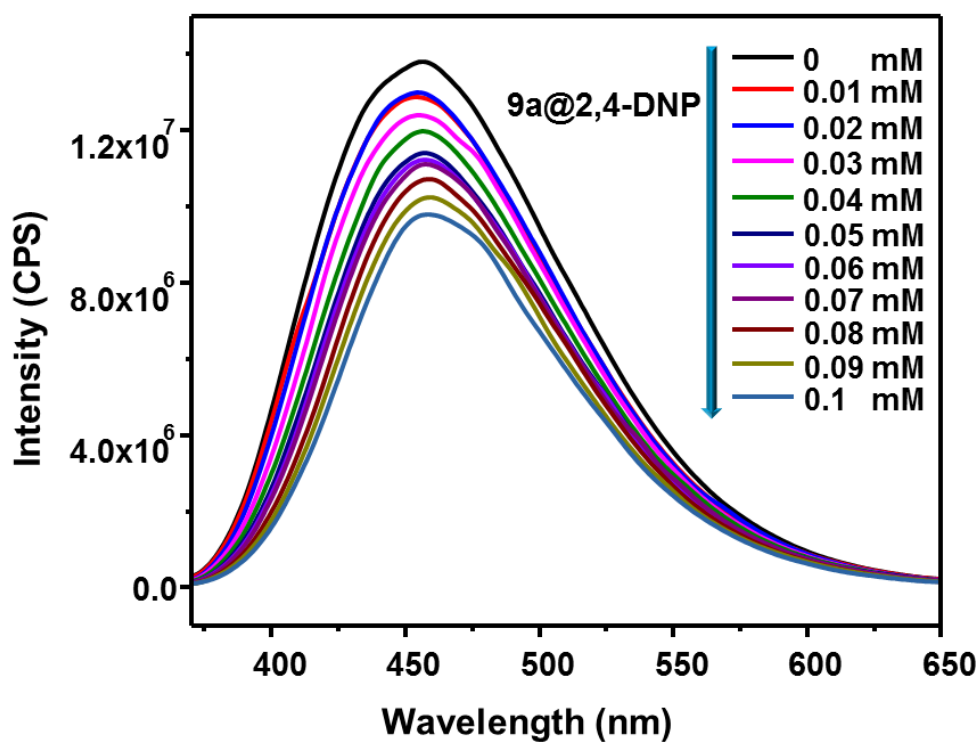
Fig. S40. Emission spectra of **9a** upon incremental addition of 2,4-dinitrophenol (2,4-DNP) solution (1 mM, 200 μL).
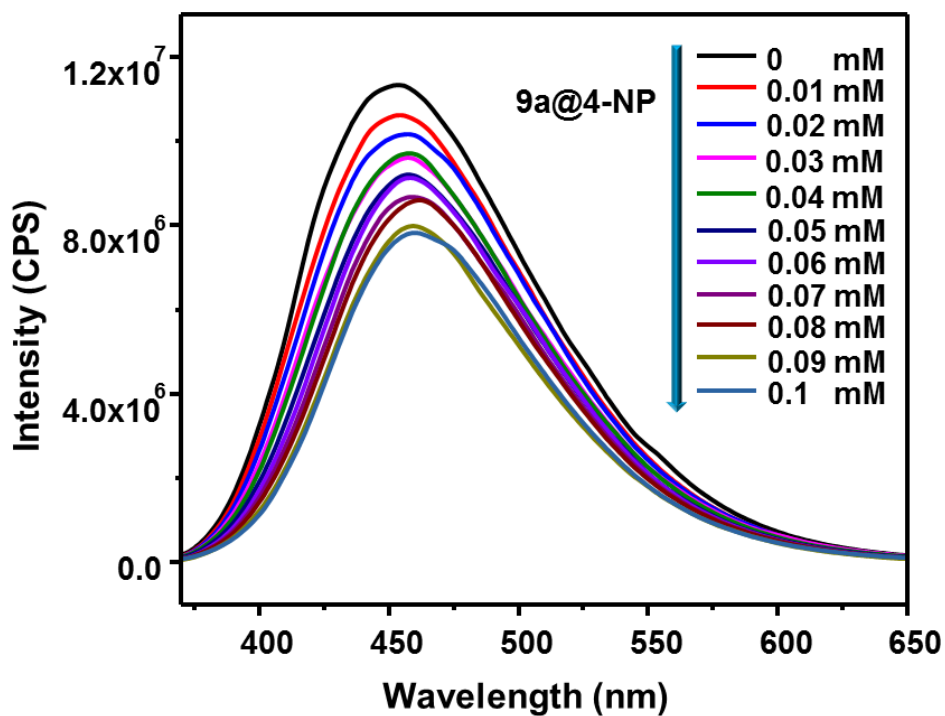
Fig. S41. Emission spectra of **9a** upon incremental addition of 4-nitrophenol (4-NP) solution (1 mM, 200 μL).
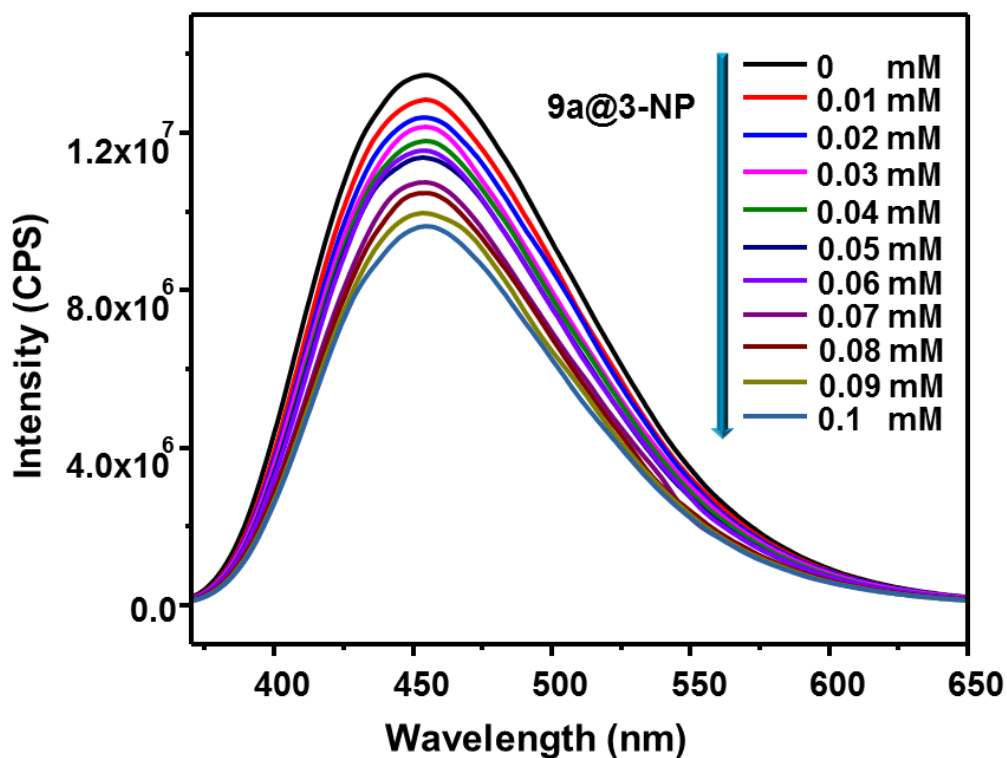
Fig. S42. Emission spectra of **9a** upon incremental addition of 3-nitrophenol (3-NP) solution (1 mM, 200 µL).
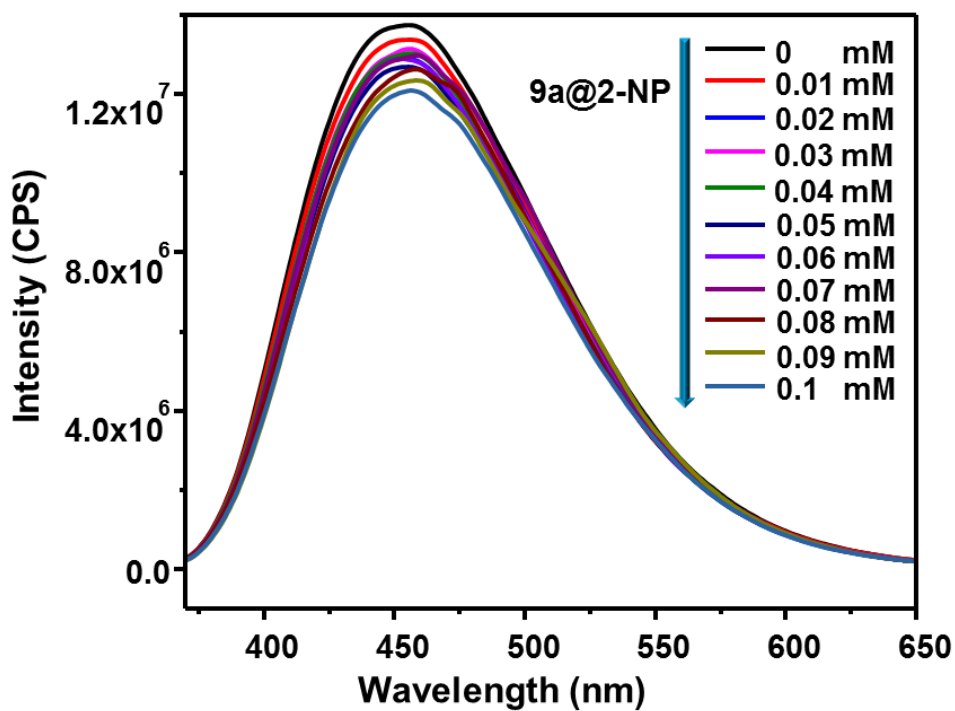
Fig. S43. Emission spectra of **9a** upon incremental addition of 2-nitrophenol (2-NP) solution (1 mM, 200 µL).
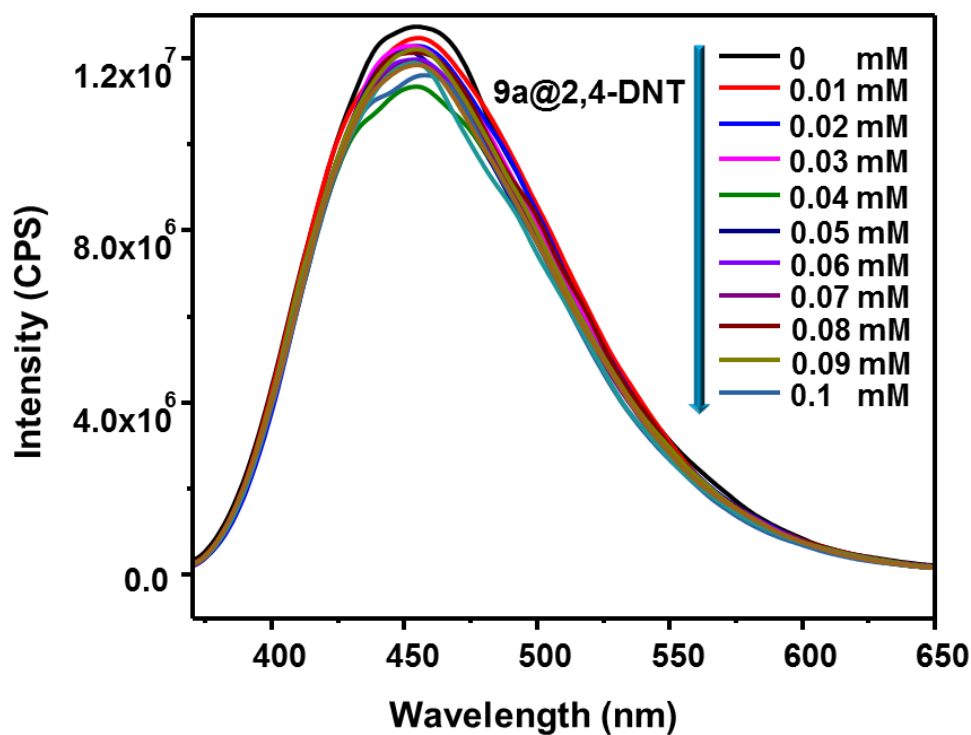
Fig. S44. Emission spectra of **9a** upon incremental addition of 2,4-dinitrotoluene (2,4-DNT) solution (1 mM, 200 μL).
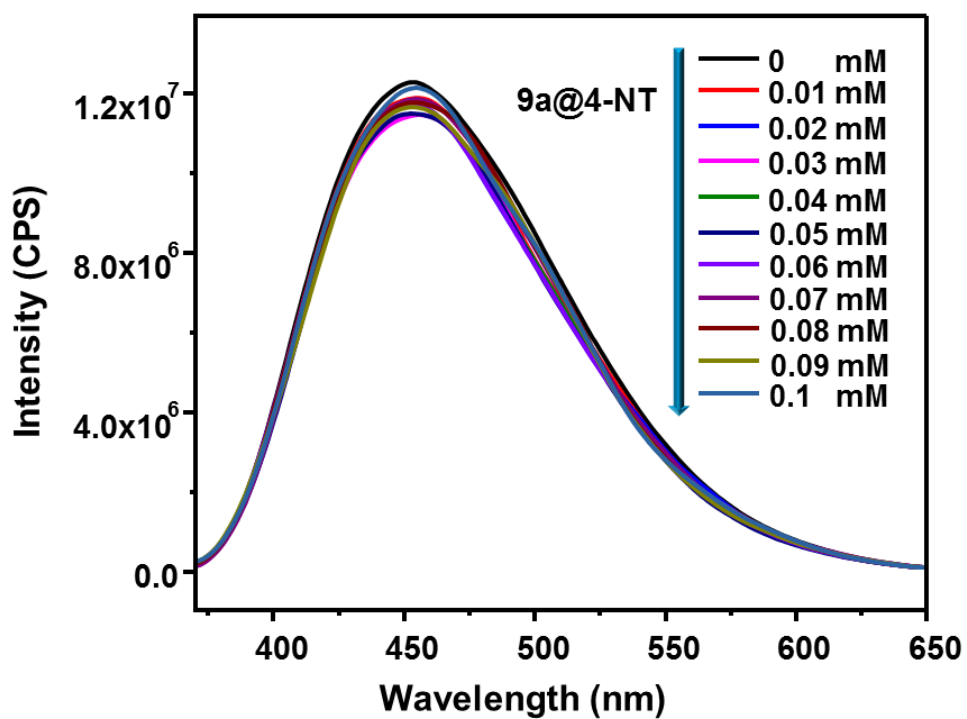
Fig. S45. Emission spectra of **9a** upon incremental addition of 4-nitrotoluene (4-NT) solution (1 mM, 200 μL).
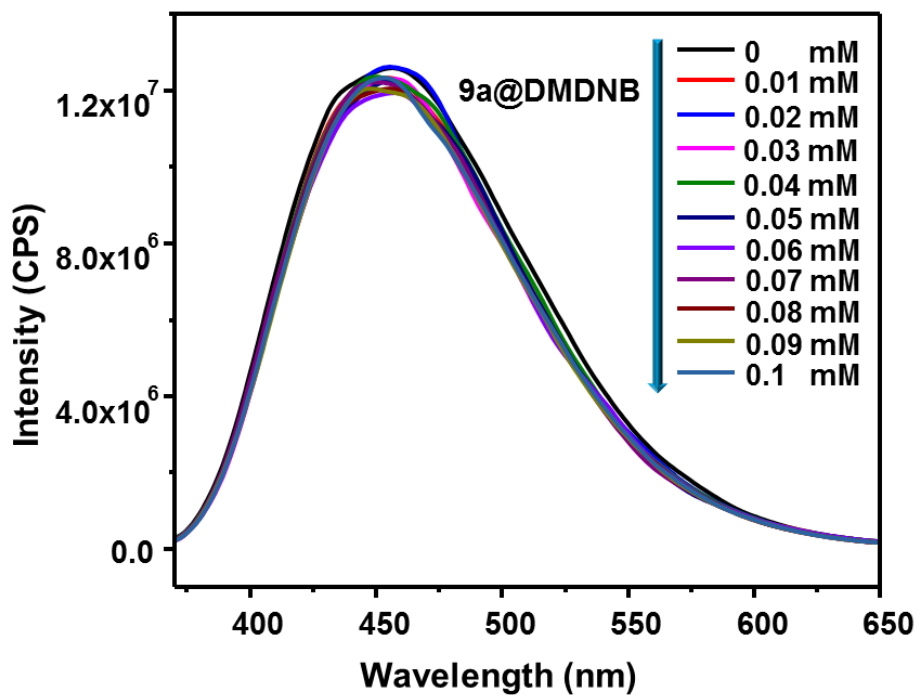
Fig. S46. Emission spectra of **9a** upon incremental addition of 2,3-dimethyl-2,3-dinitrobutane (DMDNB) solution (1 mM, 200 µL).
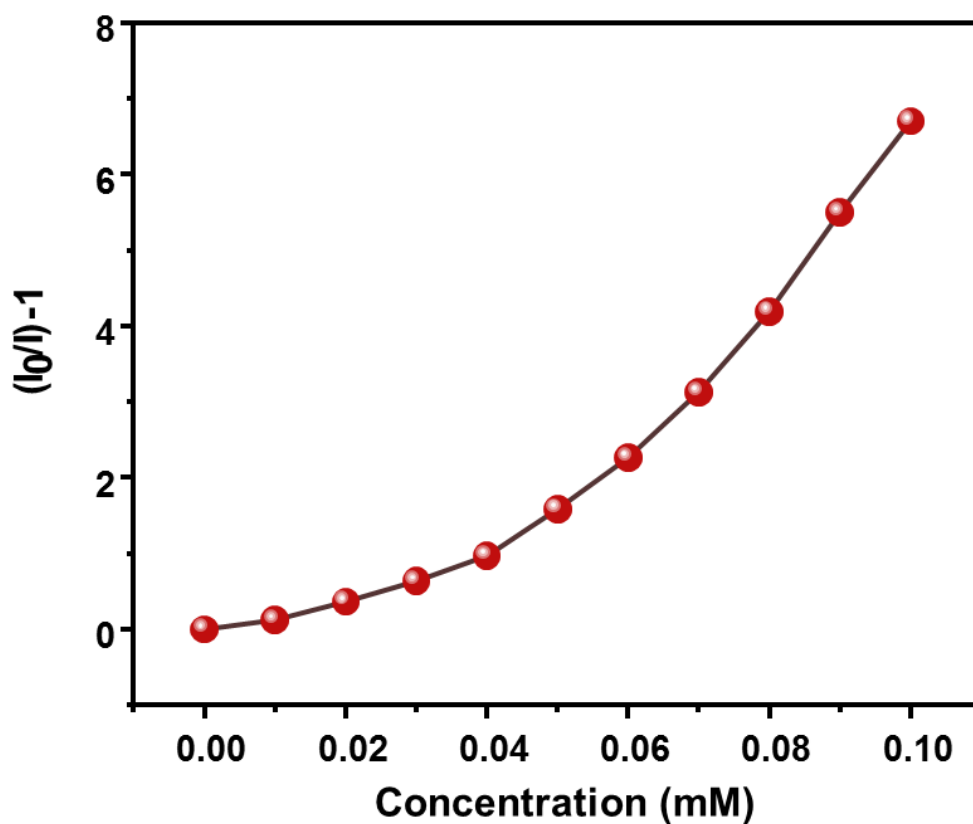
Fig. S47. The upward bent of the S–V plot for 1 mM TNP solution (0 to 200 µL).

Equation	y = a + b*x
Plot	B
Weight	No Weighting
Intercept	-0.07268 ± 0.05576
Slope	24.57034 ± 2.27654
Residual Sum of Squar	0.01555
Pearson's r	0.98737
R-Square(COD)	0.97489
Adj. R-Square	0.96652
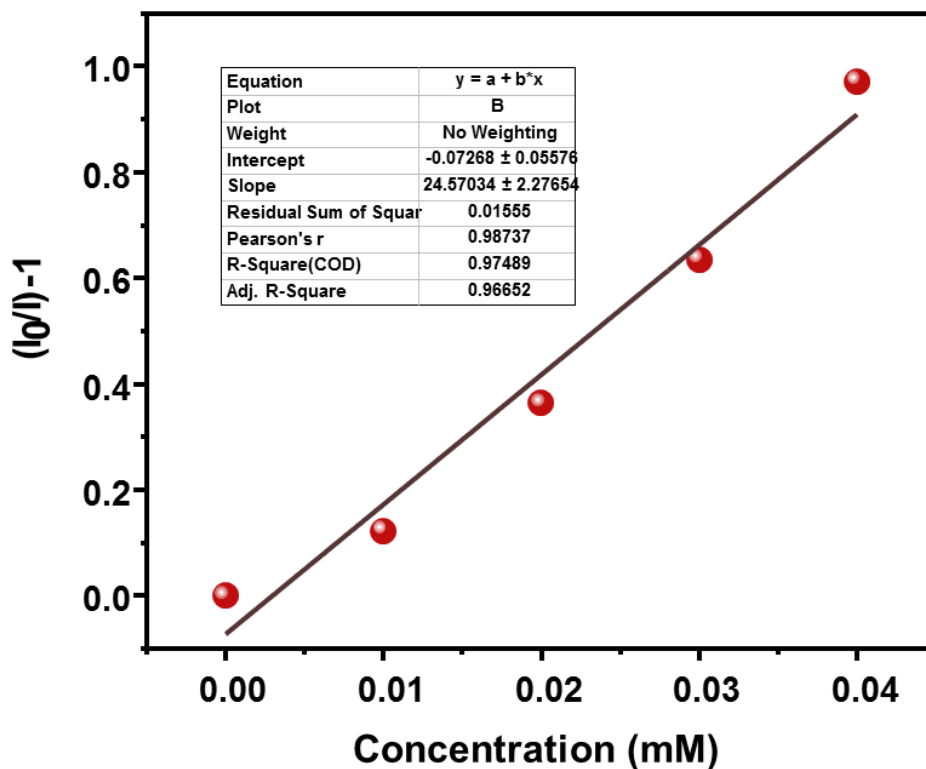
Fig. S48. Stern-Volmer (S-V) plot for 1 mM TNP solution (0 to 200 µL). The relative fluorescence intensity (I_0/I)-1 is linear with TNP concentration in the range of 0–0.04 mM.

Equation	y = a + b*x
Plot	B
Weight	No Weighting
Intercept	1.52374E7 ± 76839.
Slope	-2.67996E6 ± 12988
Residual Sum of	1.6701E11
Pearson's r	-0.9896
R-Square(COD)	0.9793
Adj. R-Square	0.977
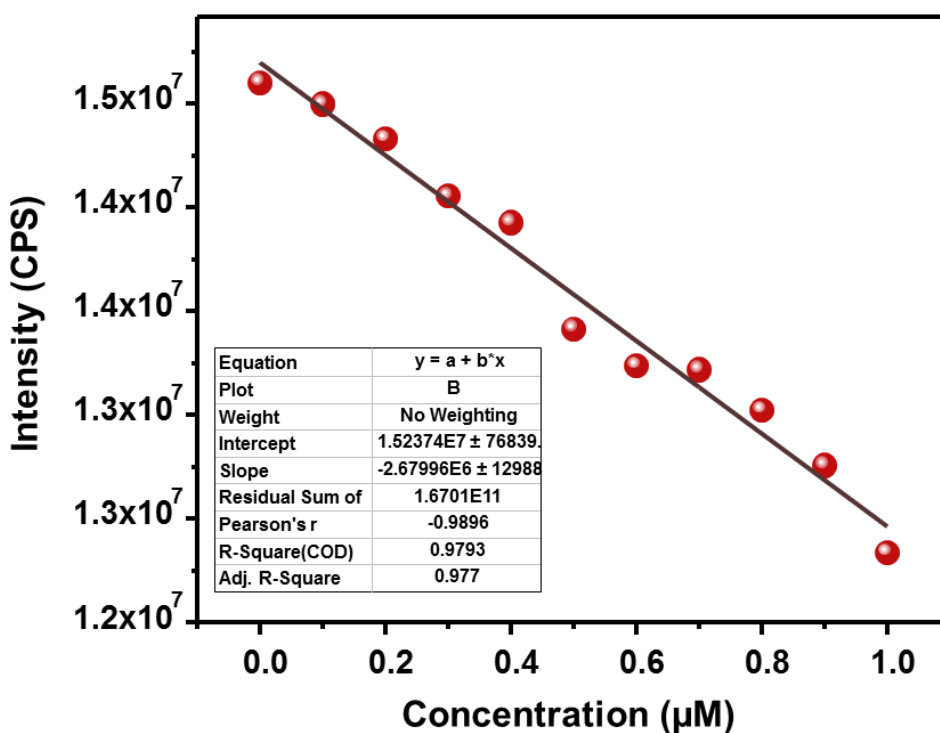
Fig. S49. Linear region of fluorescence intensity of **9a** upon addition of TNP (0 – 200 µL, 10 µM stock solution).
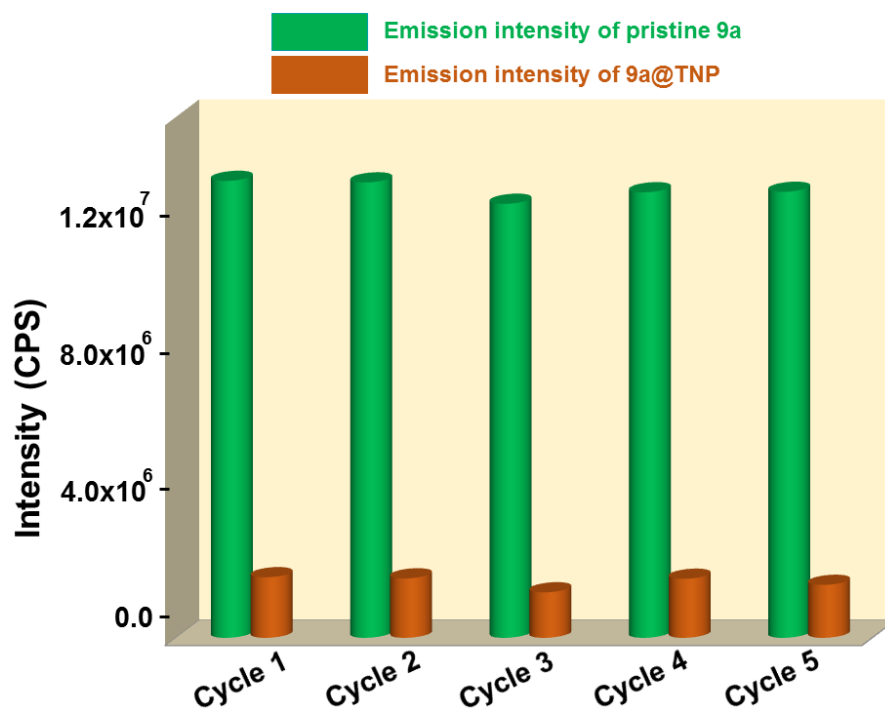
Fig. S50. Reproducibility of quenching efficiency of **9a** towards 1 mM TNP solution up to five sensing-recovery cycles.
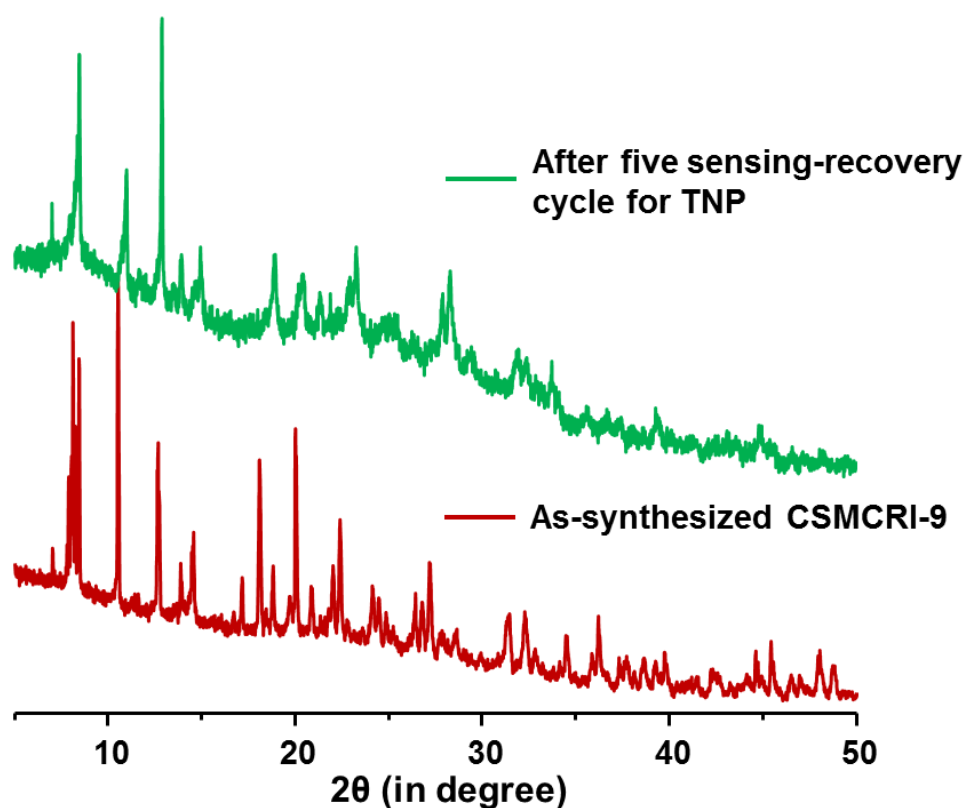
Fig. S51. PXRD patterns of **9a** obtained after five sensing-recovery cycles for TNP (1 mM), revealing that structural integrity of the framework is maintained.
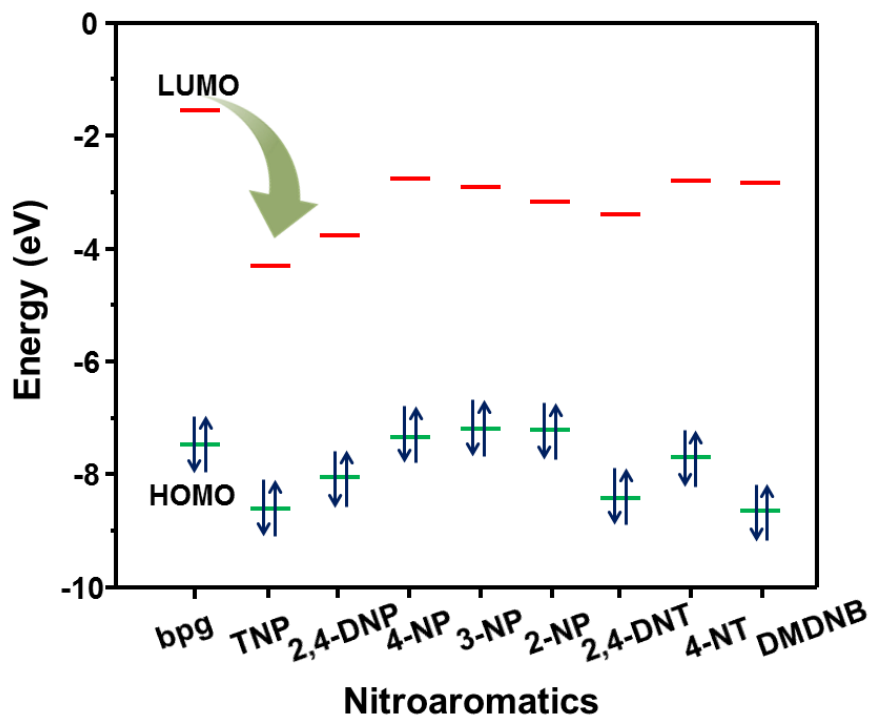
Fig. S52. HOMO–LUMO energies for bpg linker along with the studied nitroaromatic molecules.
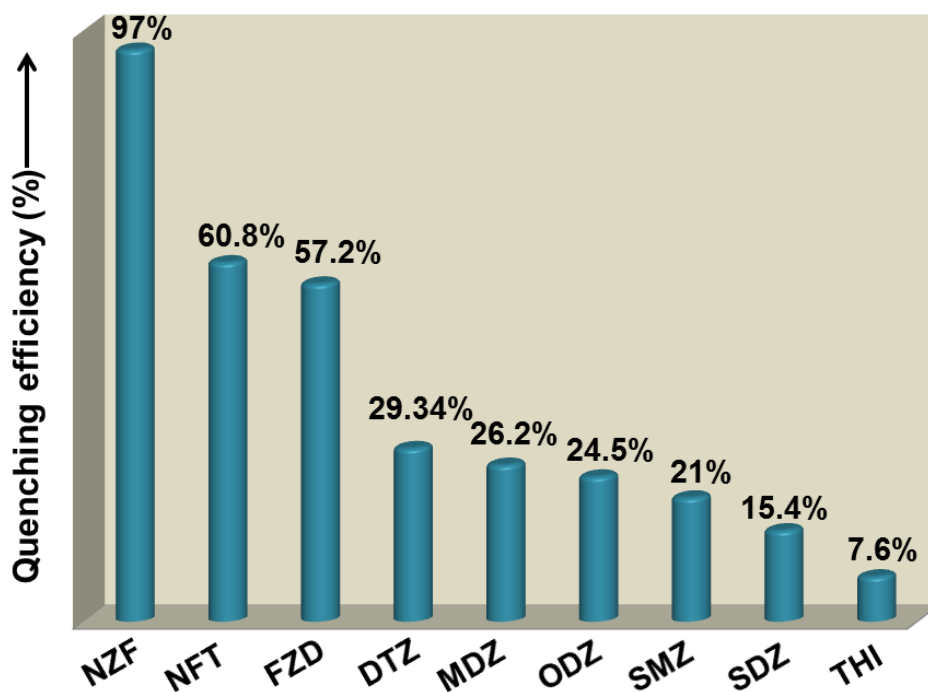
Fig. S53. Fluorescence quenching efficiency of **9a** (1 mg/ 2 mL water) towards studied antibiotics. Quenching efficiency of **9a** is calculated using equation $(I_0 - I)/I_0 \times 100\%$, where I_0 and I denotes the emission intensities before and after the addition of studied antibiotics, respectively.
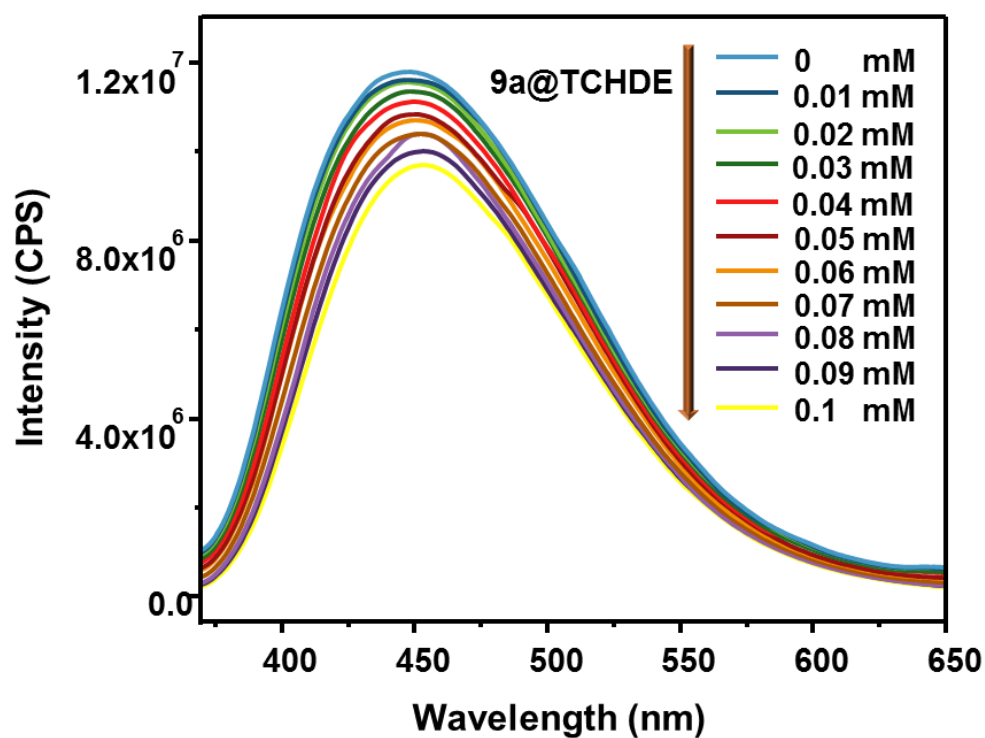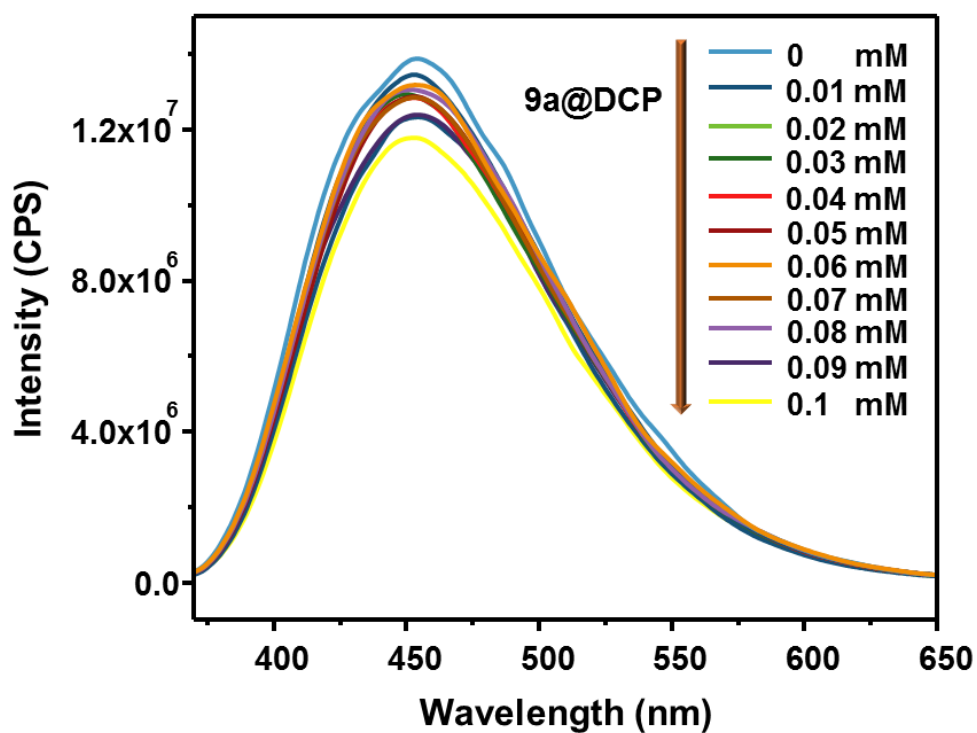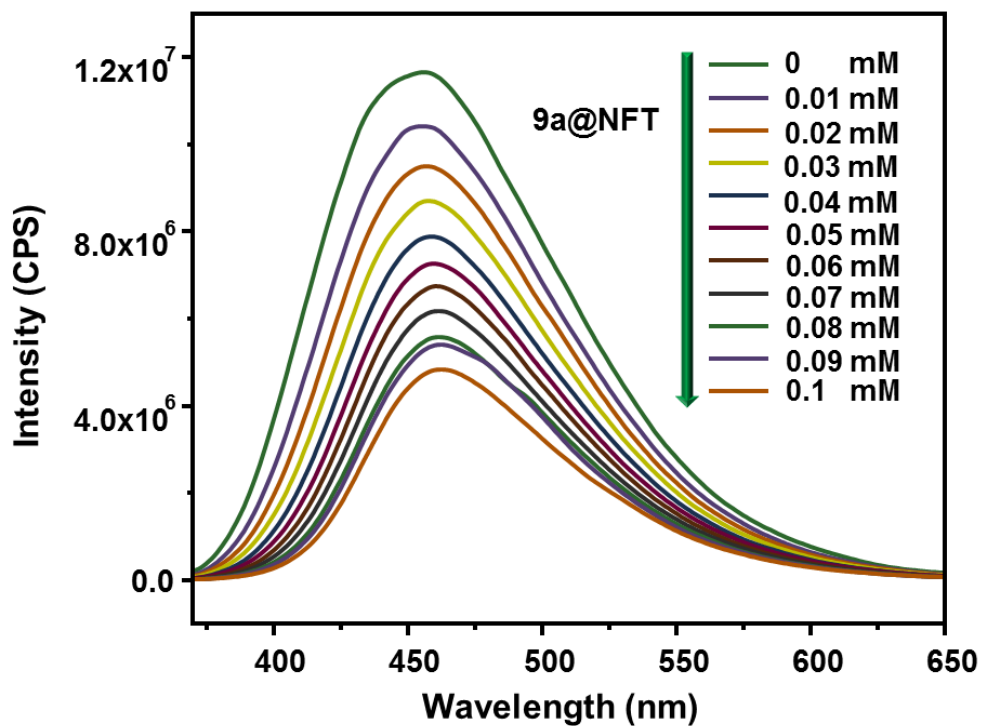
Fig. S54. Emission spectra of **9a** upon incremental addition of nitrofurantoin (NFT) solution (1 mM, 200 μL).
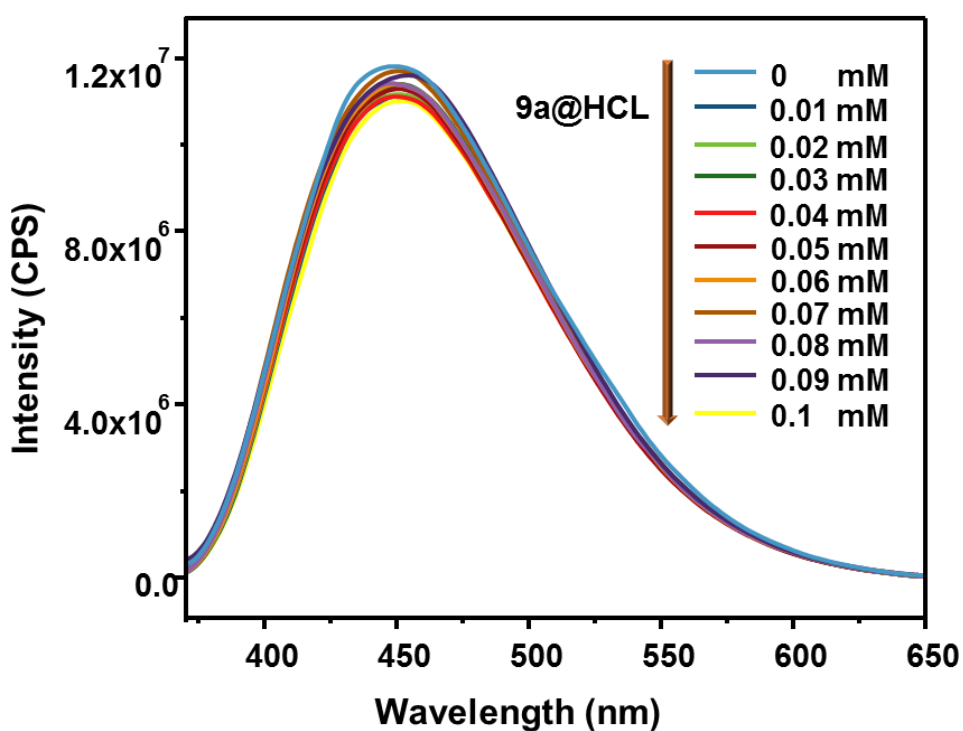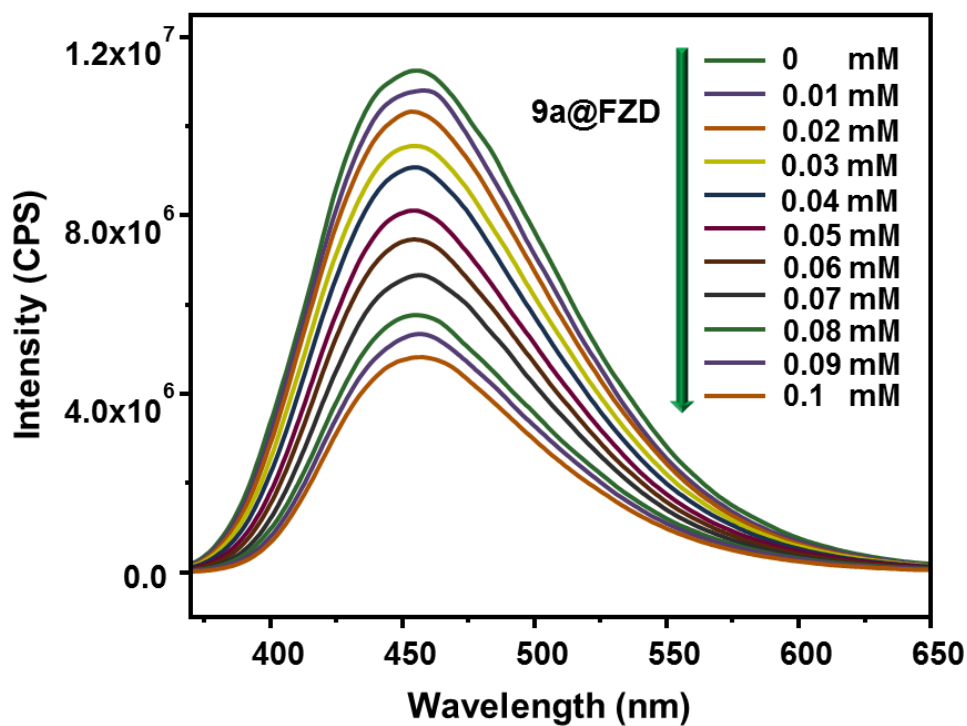

Fig. S55. Emission spectra of **9a** upon incremental addition of furazolidone (FZD) solution (1 mM, 200 μL).
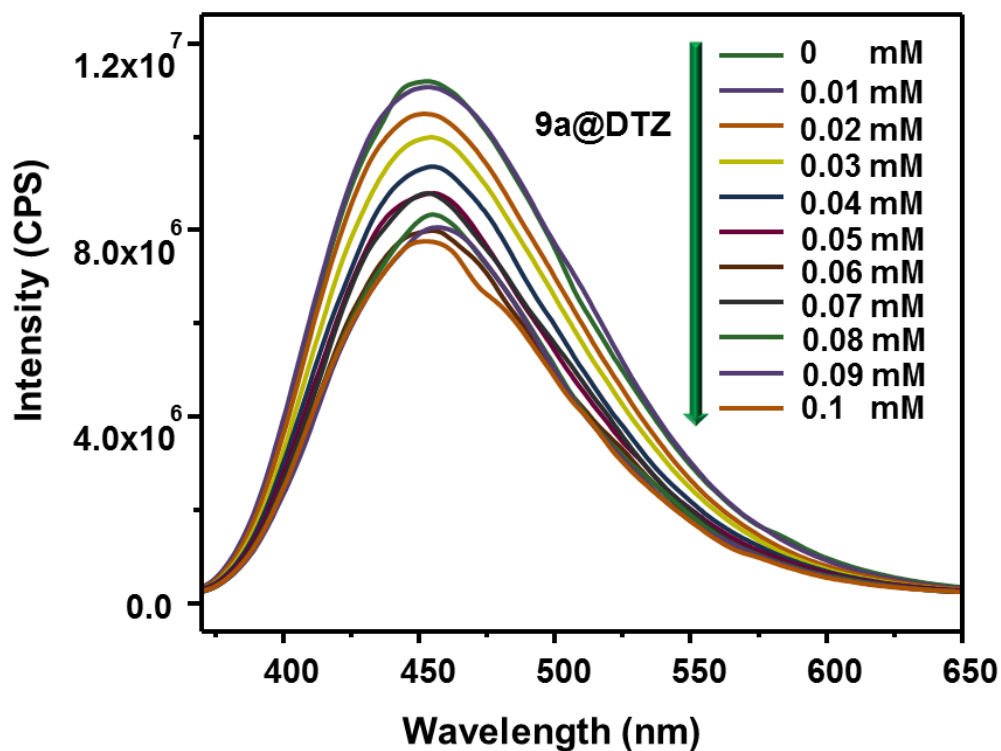
Fig. S56. Emission spectra of **9a** upon incremental addition of dimetridazole (DTZ) solution (1 mM, 200 μL).
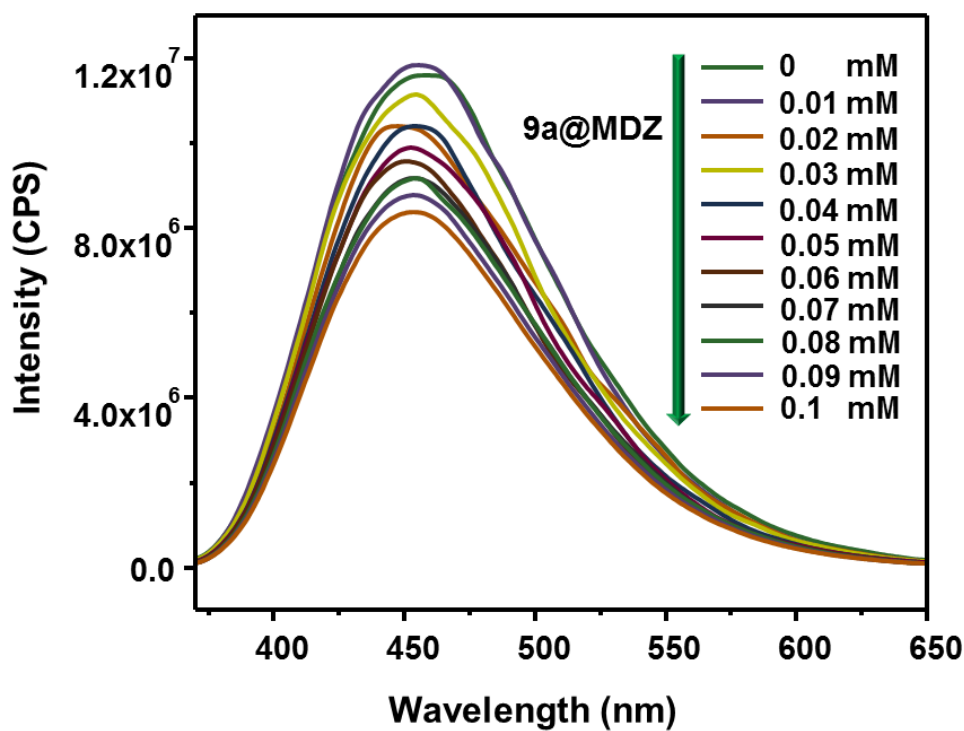
Fig. S57. Emission spectra of **9a** upon incremental addition of metronidazole (MDZ) solution (1 mM, 200 μL).
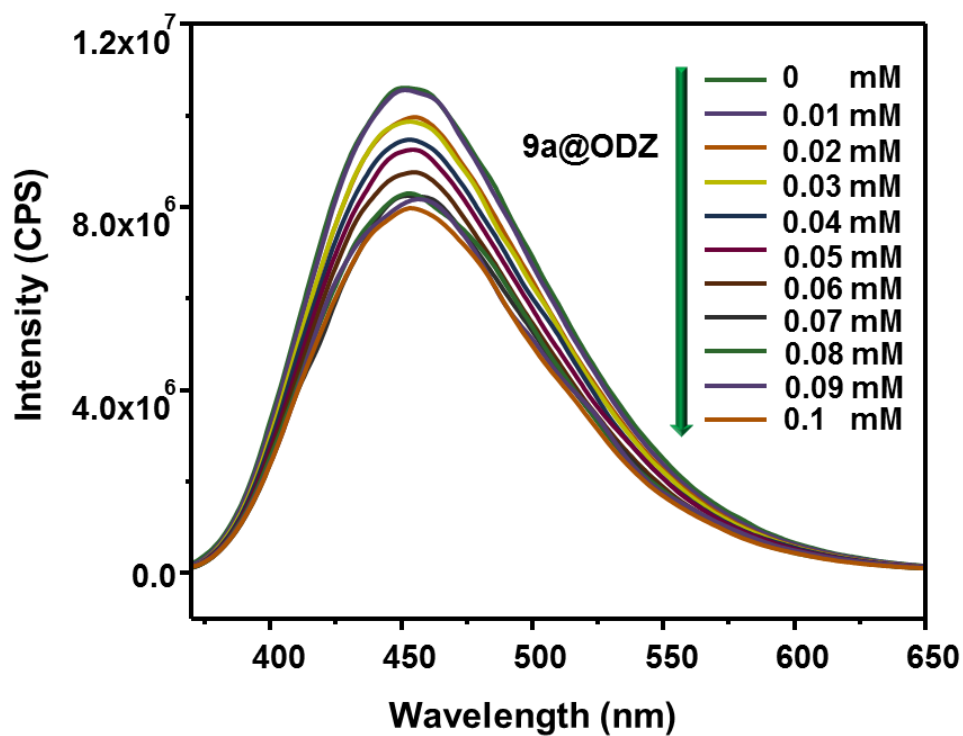
Fig. S58. Emission spectra of **9a** upon incremental addition of ornidazole (ODZ) solution (1 mM, 200 μL).
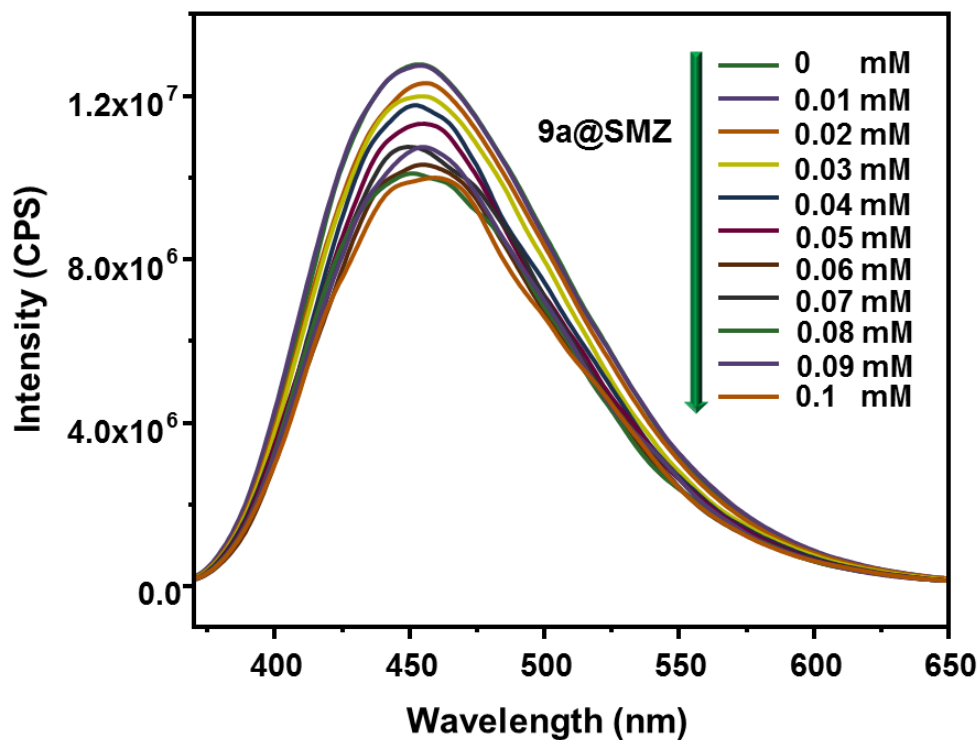
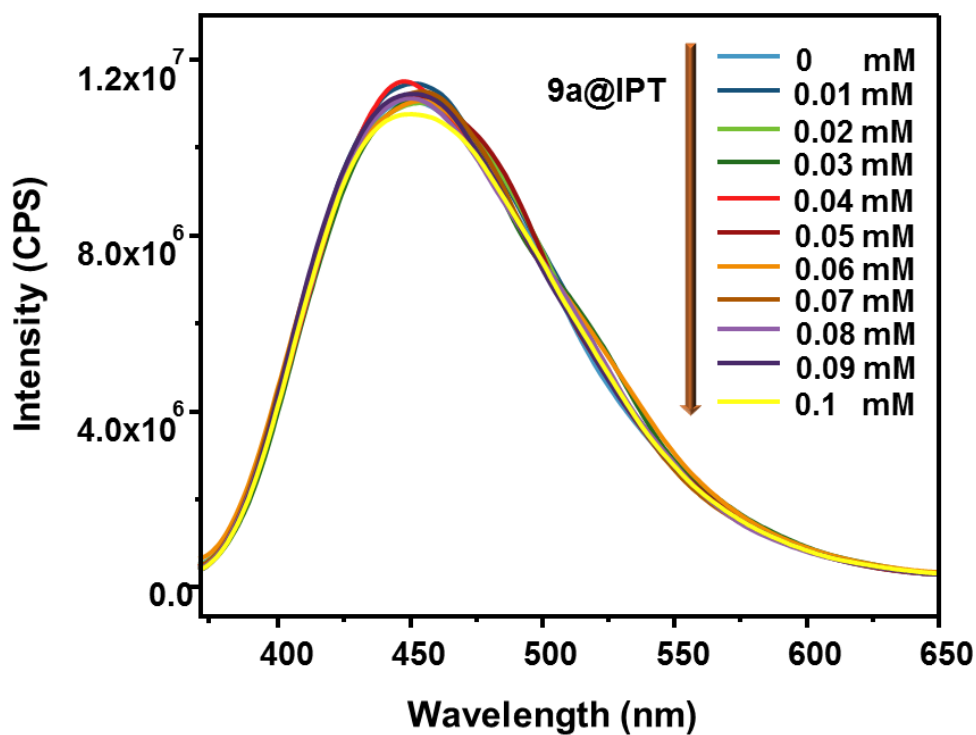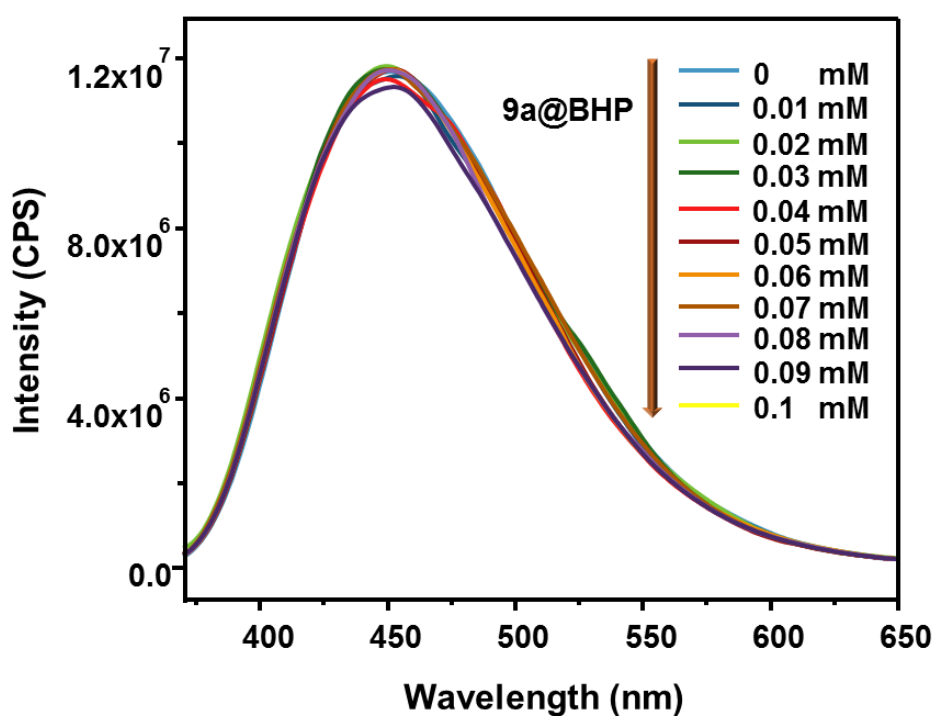**Fig. S59.** Emission spectra of **9a** upon incremental addition of sulfamethazine (SMZ) solution (1 mM, 200 μL).
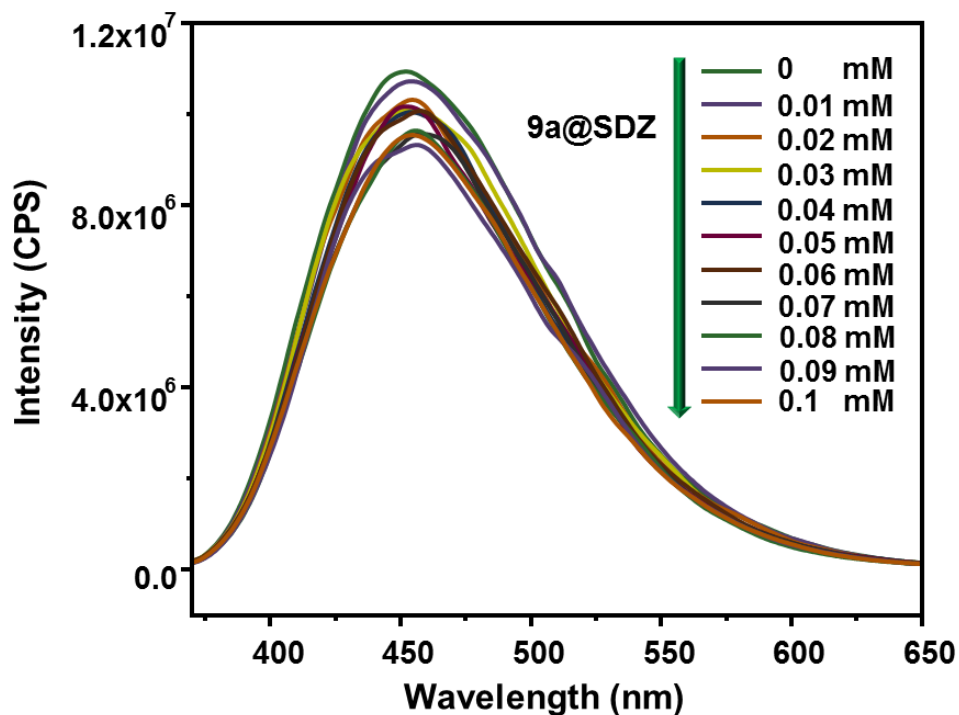
Fig. S60. Emission spectra of **9a** upon incremental addition of sulfadiazine (SDZ) solution (1 mM, 200 μL).
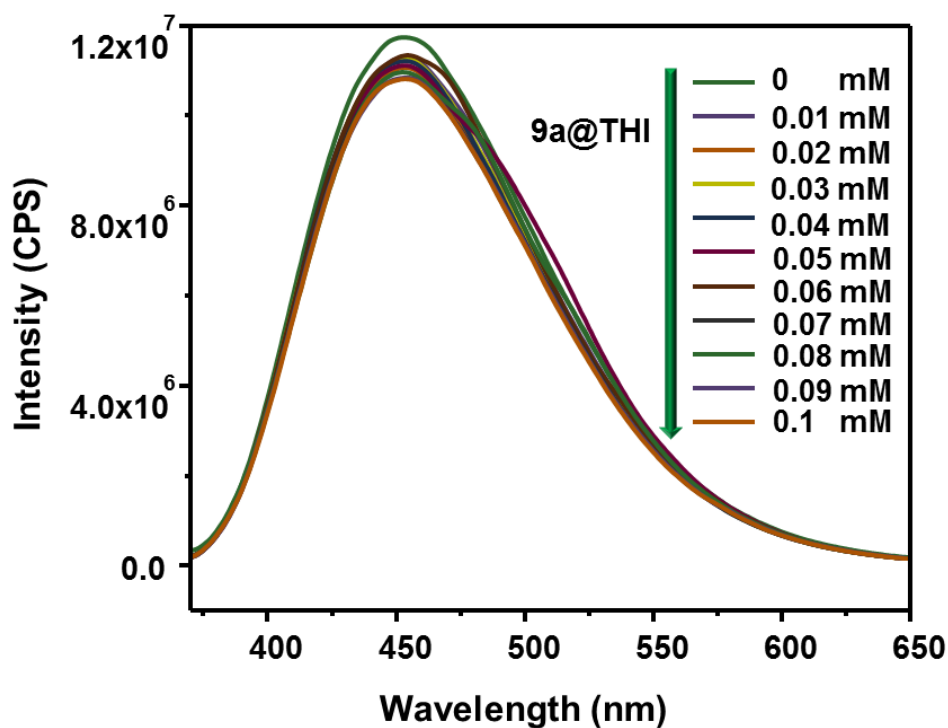
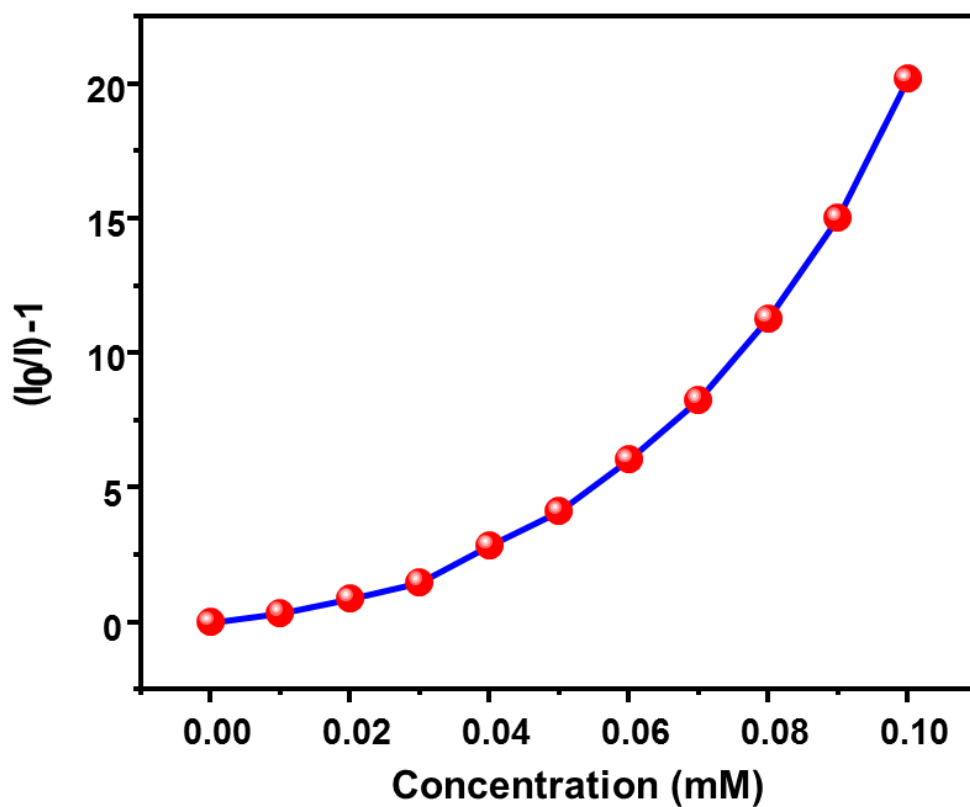**Fig. S61**. Emission spectra of **9a** upon incremental addition of thiamphenicol (THI) solution (1 mM, 200 μL).
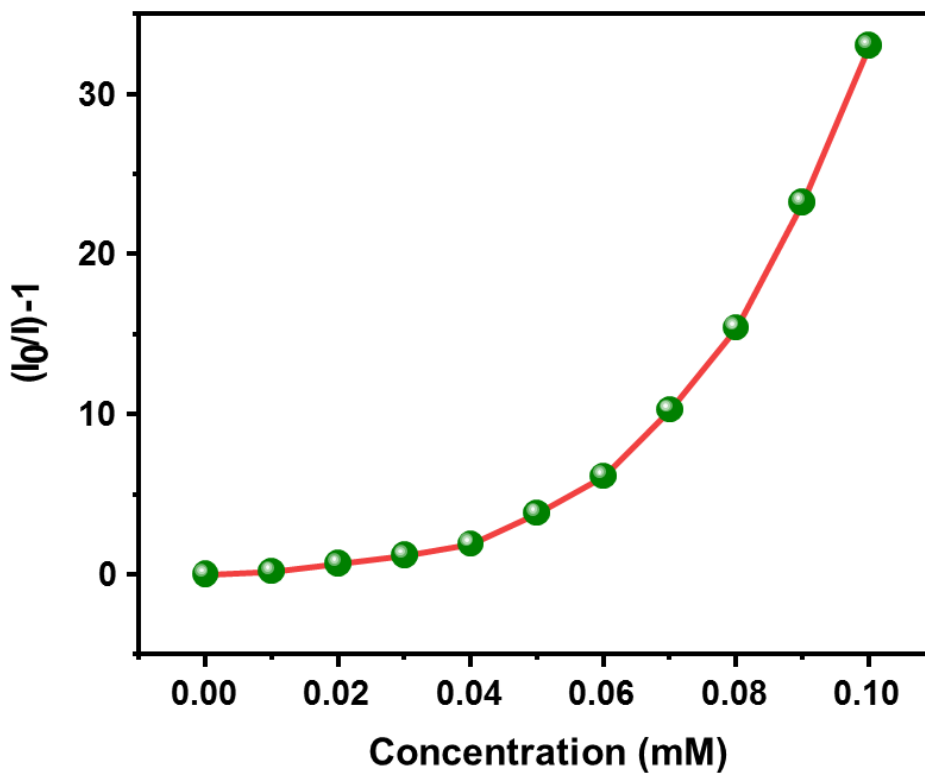
Fig. S62. The upward curvature of the S–V plot for 1 mM NZF solution (0 to 200 μL).

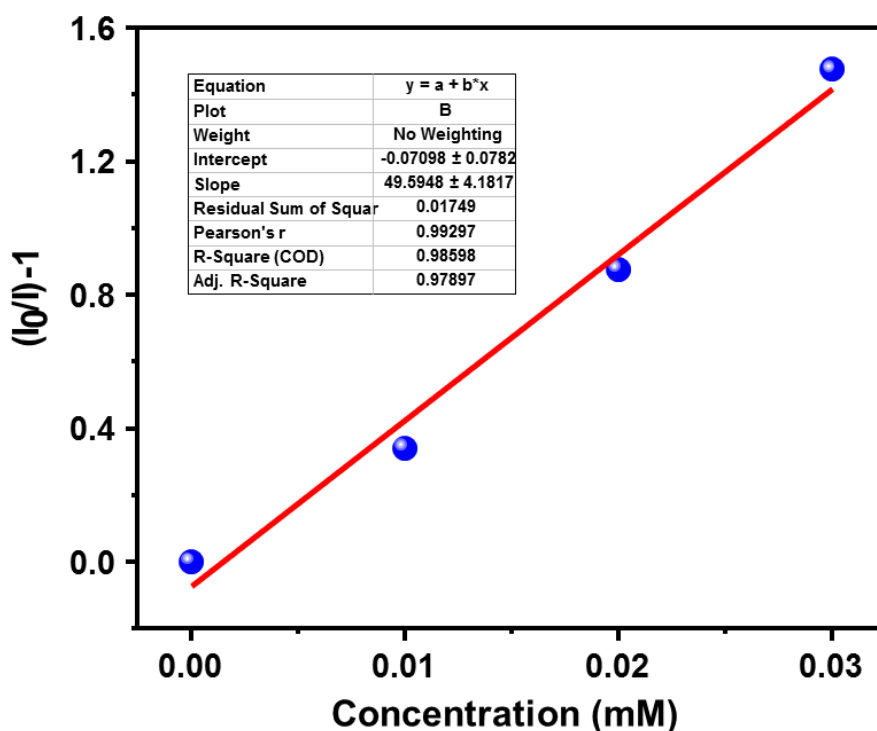| Equation	y = a + b*x
Plot	B
Weight	No Weighting
Intercept	-0.16466 ± 0.12808
Slope	48.17841 ± 5.22877
Residual Sum of Squar	0.08202
Pearson's r	0.98279
R-Square(COD)	0.96587
Adj. R-Square	0.96449
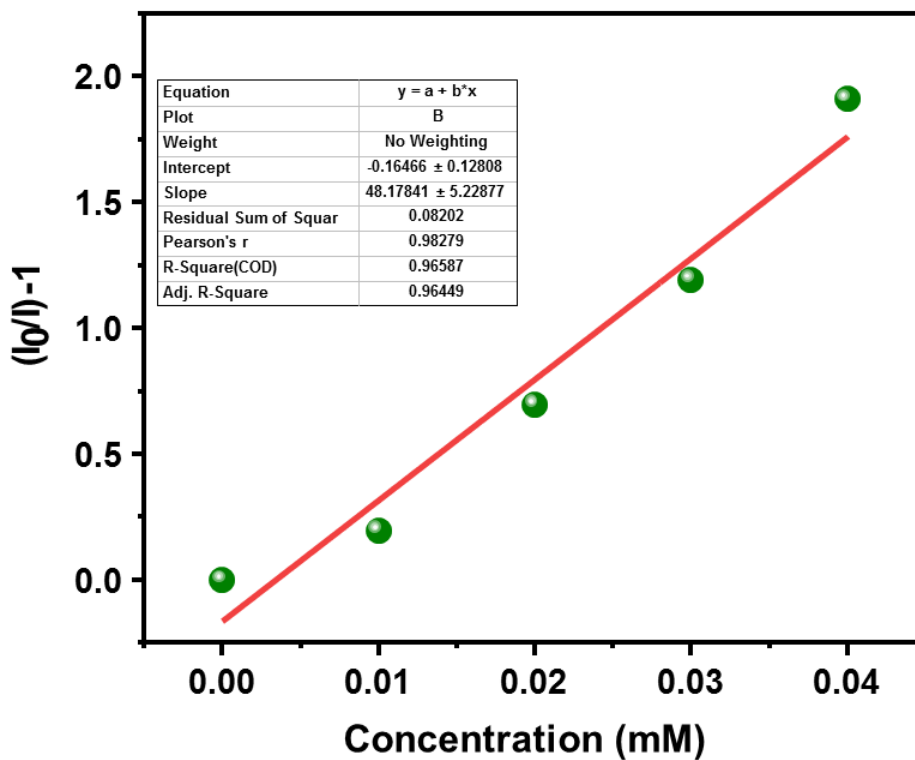
Fig. S63. Stern-Volmer (S-V) plot for 1 mM NZF solution (0 to 200 μL). The relative fluorescence intensity (I_0/I)-1 is linear with NZF concentration in the range of 0–0.04 mM.
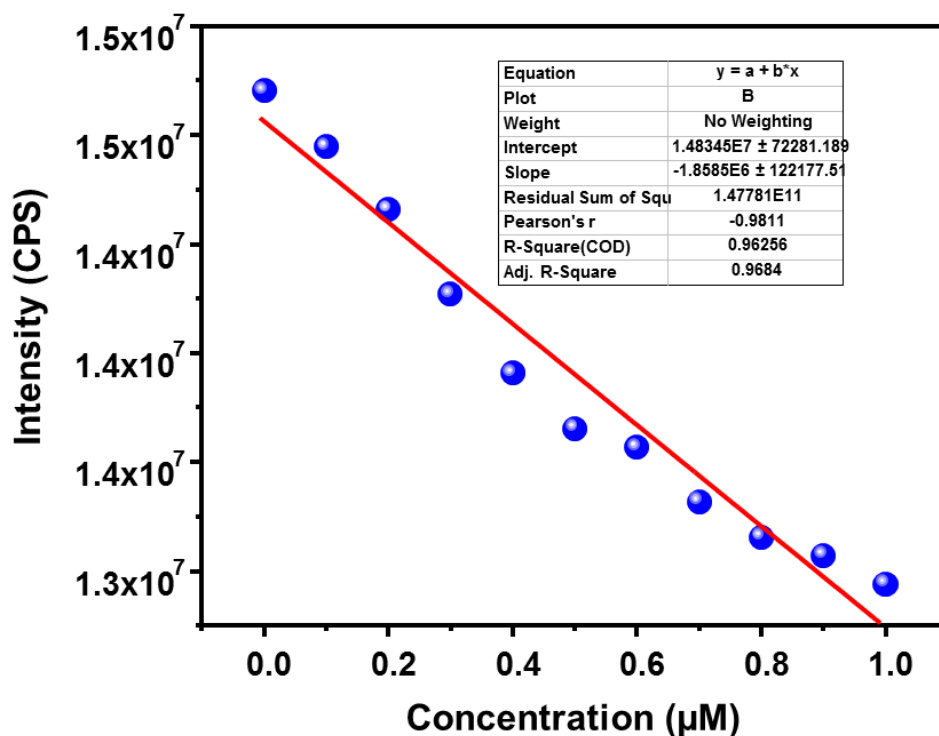
Equation	y = a + b*x
Plot	B
Weight	No Weighting
Intercept	1.39867E7 ± 37788.52853
Slope	-956324.05455 ± 63874.27134
Residual Sum of Square	4.03912E10
Pearson's r	-0.98051
R-Square(COD)	0.9614
Adj. R-Square	0.96711
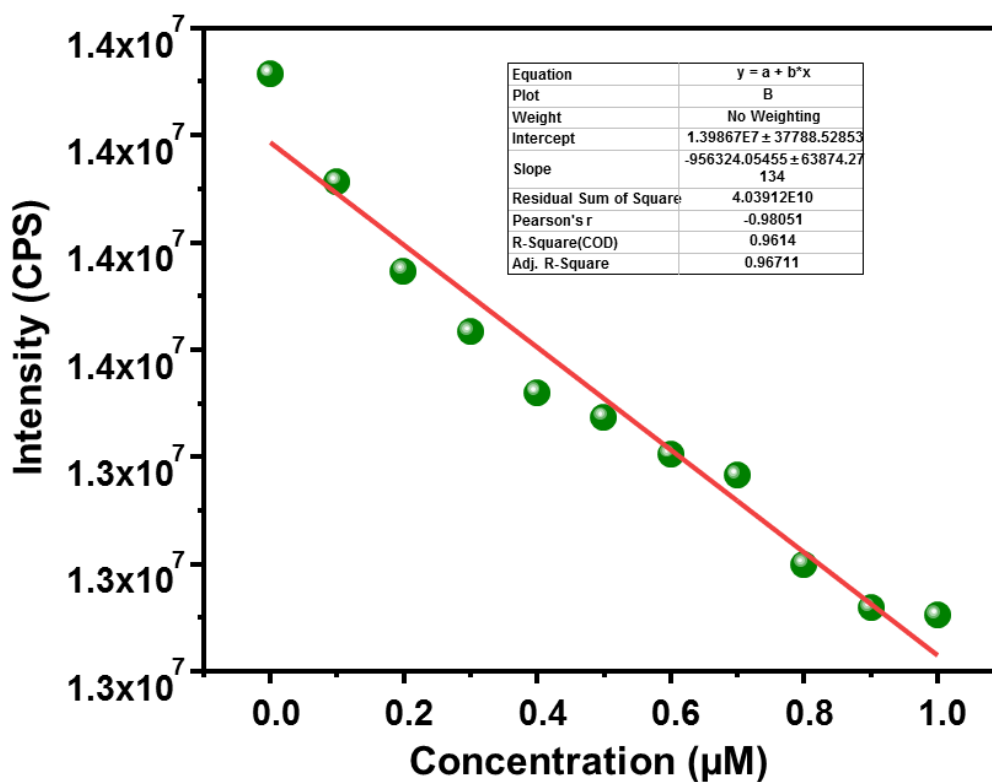
Fig. S64. Linear region of fluorescence intensity of **9a** upon addition of NZF (0 – 200 μL, 10 μM stock solution).
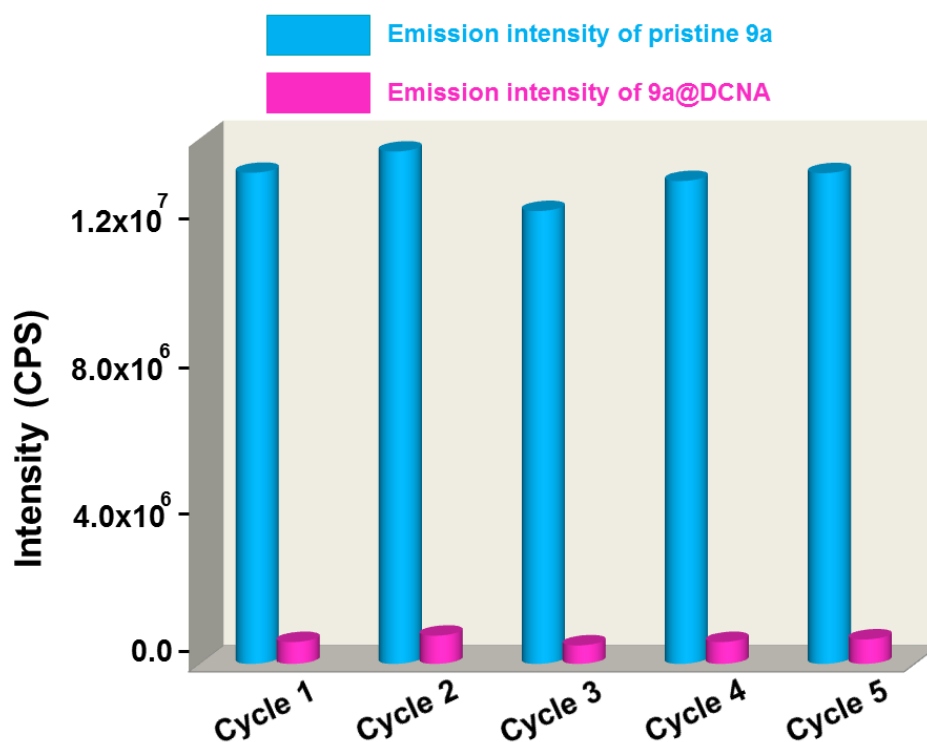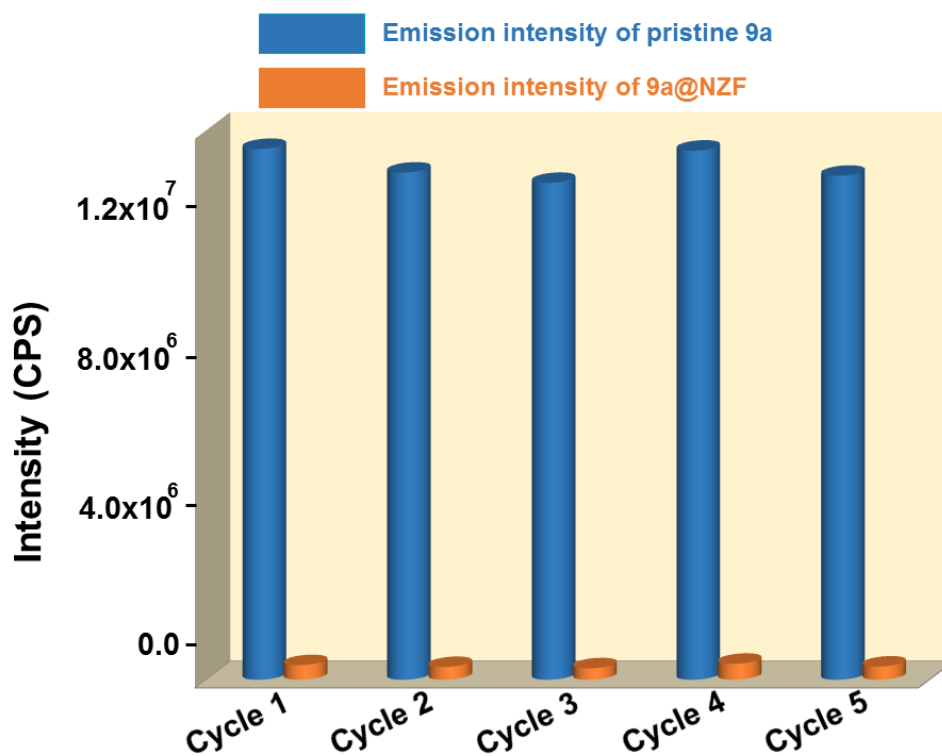

Fig. S65. Reproducibility of quenching efficiency of **9a** towards 1 mM NZF solution up to five sensing-recovery cycles.
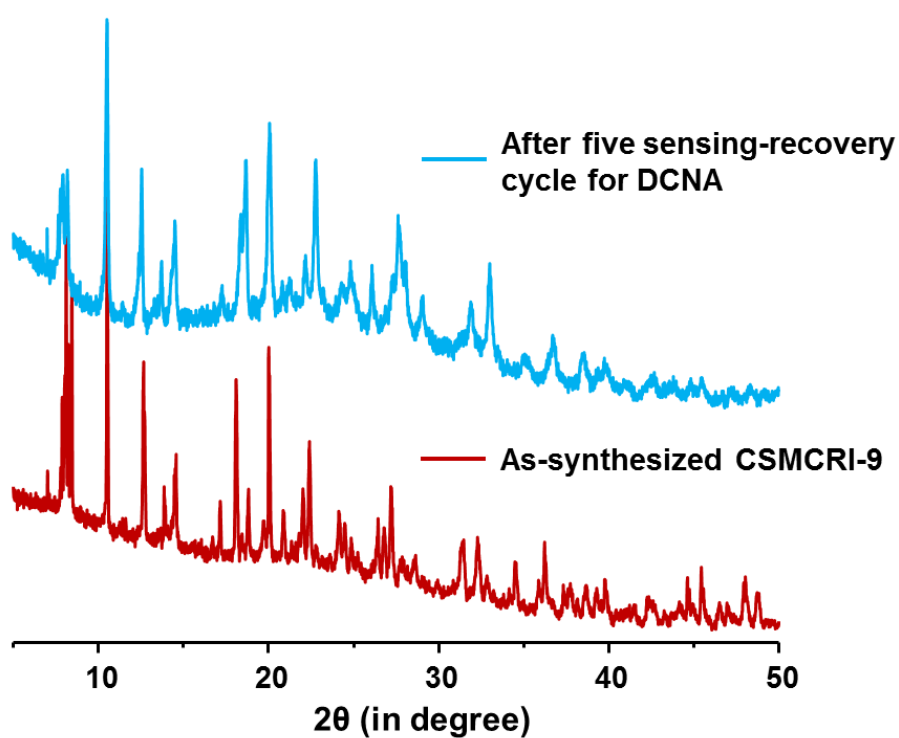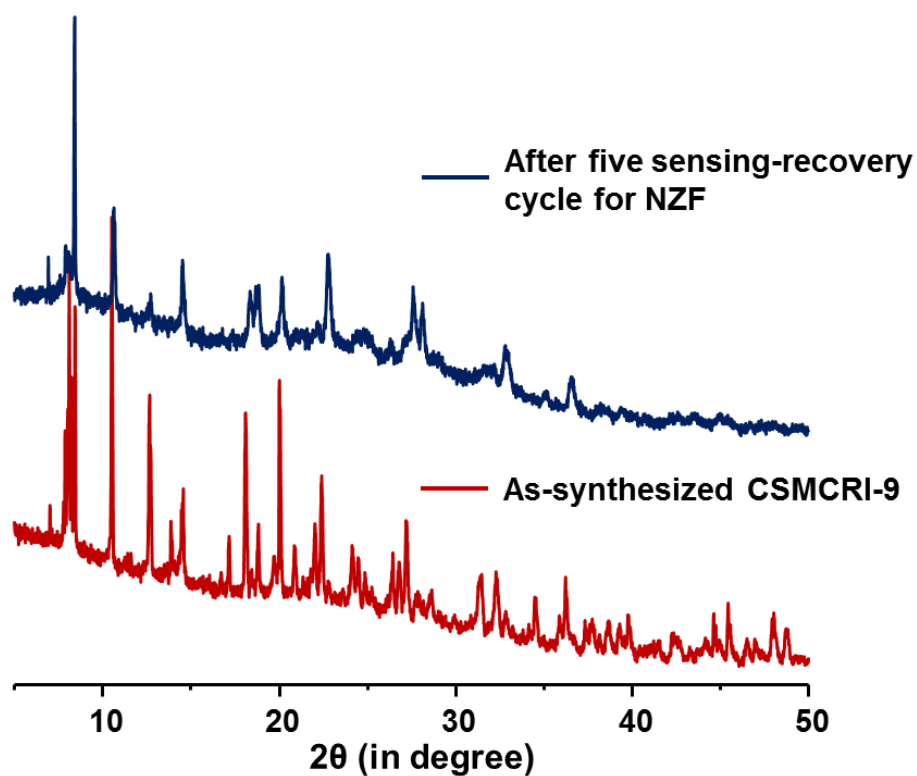
Fig. S66. PXRD patterns of **9a** obtained after five sensing-recovery cycles for NZF (1 mM), revealing that structural integrity of the framework is maintained.
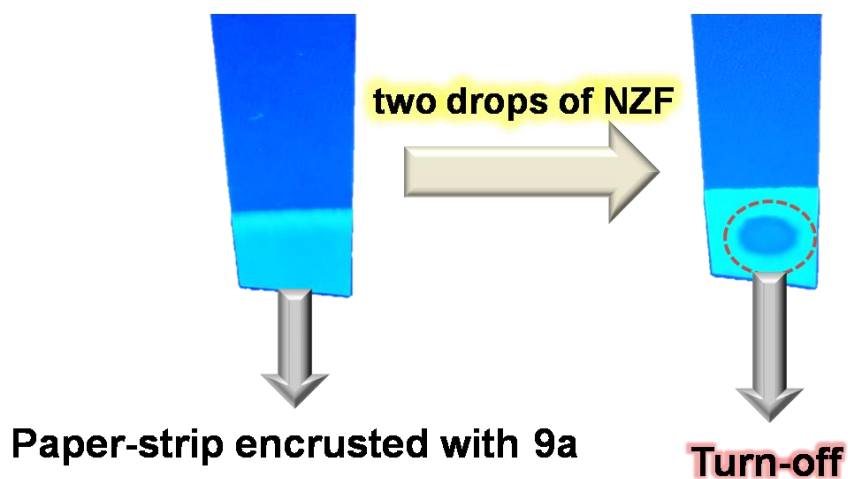

Fig. S67. Photographs of paper-strips encrusted with **9a** and after addition of NZF solution, under 365 nm UV-light.
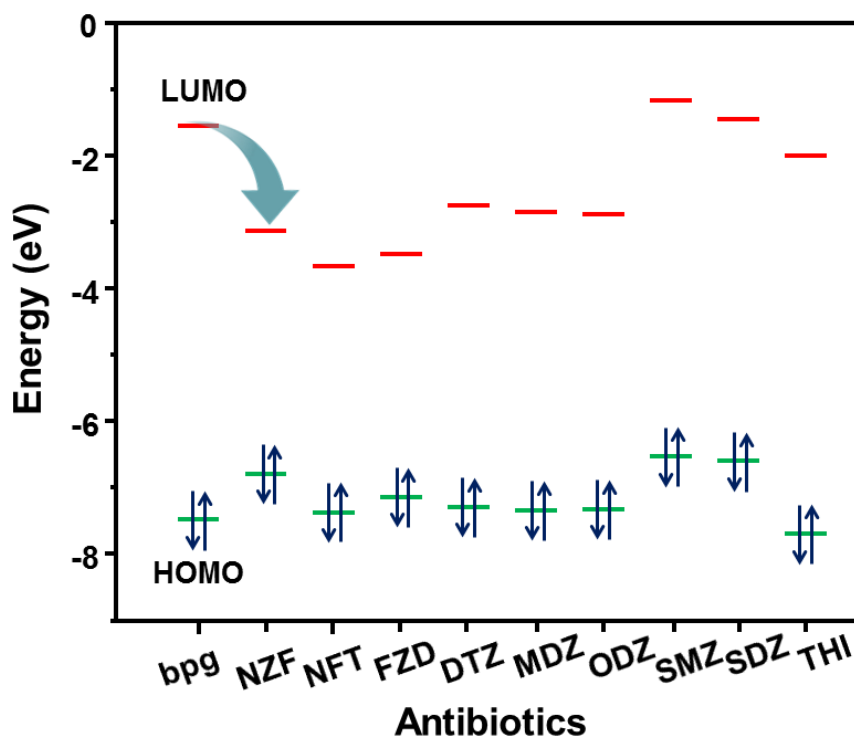
Fig. S68. HOMO–LUMO energies for bpg linker along with the studied antibiotic molecules.
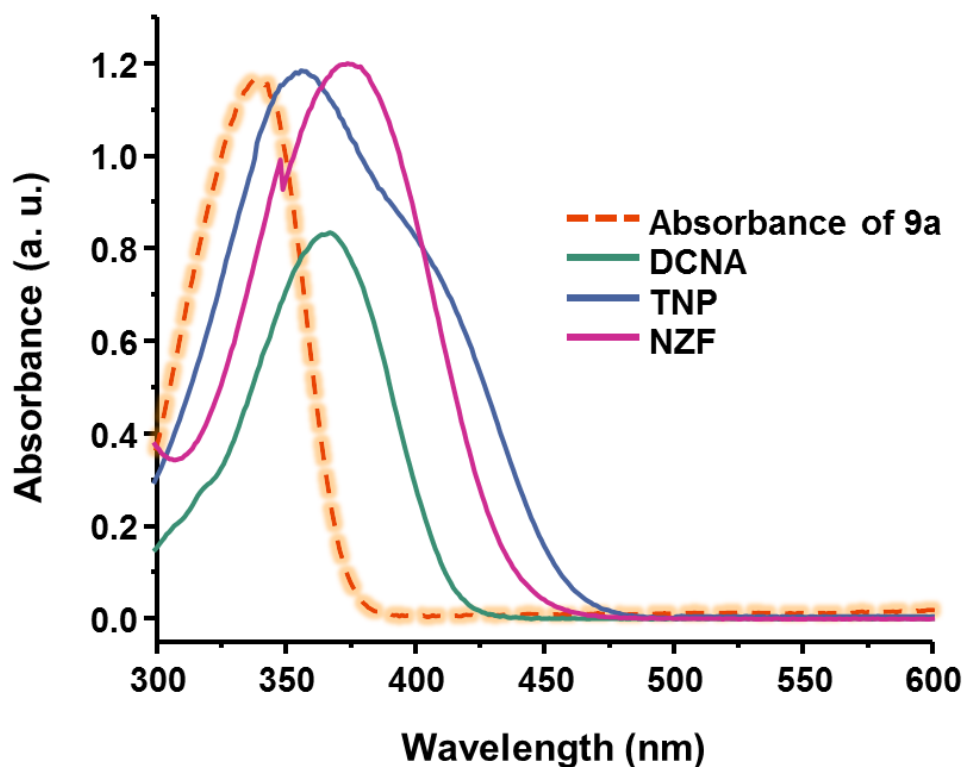
Fig. S69. Spectral overlap of the absorption spectrum of **9a** with the absorption spectra of the DCNA, TNP and NZF; revealing competitive energy absorption mechanism in luminescence quenching.

Table S1. Crystal data and refinement parameters for **CSMCRI-9**

Identification code	**CSMCRI-9**
Empirical formula	$C_{27}H_{18}Cd_{1.5}N_2O_{7.5}$
Formula weight	659.07
Temperature/K	300.15
Crystal system	monoclinic
Space group	$C2/c$
a/Å	13.1243(12)
b/Å	25.790(2)
c/Å	20.1869(18)
α/°	90
β/°	106.870(3)
γ/°	90
Volume/Å^3	6538.7(10)
Z	8
ρ_{calc}g/cm^3	1.3389
μ/mm^{-1}	1.025
F(000)	2599.6
Crystal size/mm^3	0.34 × 0.158 × 0.12
Radiation	Mo Kα (λ = 0.71073)
2Θ range for data collection/°	4.62 to 66.48
Index ranges	-20 ≤ h ≤ 20, -39 ≤ k ≤ 39, -30 ≤ l ≤ 31
Reflections collected	65349
Independent reflections	12443 [R_{int} = 0.0617, R_{sigma} = 0.0483]
Data/restraints/parameters	12443/0/345
Goodness-of-fit on F^2	1.061
Final R indexes [I>=2σ (I)]	R_1 = 0.0505, wR_2 = 0.1440
Final R indexes [all data]	R_1 = 0.0799, wR_2 = 0.1753
Largest diff. peak/hole / e Å^{-3}	1.77/-1.35

Alert level A

PLAT410_ALERT_2_A Short Intra H...H Contact H010 ..H010 . 1.62 Ang. 2-x,y,3/2-z = 2_756
Check

Alert level B

PLAT213_ALERT_2_B Atom C60 has ADP max/min Ratio ..... 4.2 prolat
PLAT213_ALERT_2_B Atom C62 has ADP max/min Ratio ..... 4.3 prolat
PLAT220_ALERT_2_B NonSolventResd 1 C Ueq(max) / Ueq(min) Range 7.0 Ratio
PLAT241_ALERT_2_B High MainMolUeq as Compared to Neighbors of O1 Check

PLAT241_ALERT_2_B High MainMolUeq as Compared to Neighbors of C60 Check

PLAT241_ALERT_2_B High MainMolUeq as Compared to Neighbors of C62 Check

PLAT242_ALERT_2_B Low MainMolUeq as Compared to Neighbors of Cd1 Check

PLAT242_ALERT_2_B Low MainMolUeq as Compared to Neighbors of C00Z Check

PLAT420_ALERT_2_B D-H Without Acceptor O7 --H7A. Please Check

Explanation: All these alerts have been generated probably due to some disorder in the structure.

Determination of formula & solvent composition of CSMCRI-9 from PLATON Squeeze and Thermogravimetric analysis data:

From the TGA plot of as-synthesized **CSMCRI-9**, the observed mass loss is 29.61 %

From PLATON Squeeze program void electron count / unit cell comes out to be 165

As the asymmetric unit is electrically neutral and, during the synthesis, DMA and water were used as solvents; so the void space should be occupied by these lattice solvent molecules.

Now, formula of the asymmetric unit excluding all guests is $[Cd_{1.5}(TCA)(bpg)_{0.5}(H_2O)]$, and mass of this asymmetric unit is 658.61

Table S2. Number of electrons and molecular mass of guest molecules associated with **CSMCRI-9** for determination of solvent composition and molecular formula

	Dimethyl acetamamide (DMA)	Water
No. of electrons	48	10
mass	87	18

Considering the above mentioned number of electrons, the best possible combination of solvent molecules for **CSMCRI-9** could be $[Cd_{1.5}(TCA)(bpg)_{0.5}(H_2O)] \cdot 3DMA \cdot 2H_2O$

The total number of electrons contributed by lattice solvent molecules will be [(48×3) + (10×2)] = 164, which is in well agreement with the PLATON result and thus validates the above formula.

The aforementioned combination was further cross-checked from TGA analysis.

Total mass loss due to solvents is [(87×3) + (18×2)] = 297

Therefore total mass of **CSMCRI-9** including all the guests is (658.61+297) = 955.61

So mass loss due to solvents is [(297/955.61)×100] % = 31.07 %, which is in good agreement with that of the TGA result.

Table S3. A comparison for BET surface area and CO_2 adsorption capacity of some well reported MOFs at 1 bar

Sl. No.	MOF	BET Surface Area (m²/g)	Uptake capacity (273 K)	Uptake capacity (298 K)	References
1.	SNU-5	–	38.5wt% 8.75 mmol/g	–	*Angew.Chem.Int.Ed* **2008**,*47*, 7741 −7745
2.	PCN-124	1372	28.6wt% 6.5 mmol/g	–	*Chem. Commun.* **2012**, *48*, 9995-9997
3.	Cu-NTTA	3931	22.7 wt% 5.15 mmol/g	12.86 wt% 2.92 mmol/g	*ACS Appl. Mater. Interfaces* **2016**, *8*, 31746−31756
4.	NUM-3a	2111.2	22.19wt% 5.04 mmol/g	16.30 wt% 3.70 mmol/g	*ACS Appl. Mater. Interfaces* **2017**, *9*, 26177−26183
5.	CPF-6	599	19.25wt% 4.37 mmol/g	–	*J. Am. Chem.Soc.* **2012**, *134*, 784−787
6.	IRMOF-9	1904	7.85 wt% 1.78 mmol/g	–	*Chem. Commun.***2014**, *50*, 3238-3241 & *J. Am. Chem. Soc.* **2006**, *128*, 1304-1315
7.	TTF-4	1172	13.3 wt% 3.02 mmol/g	7.54 wt% 1.71 mmol/g	*Chem. Commun.* **2016**, *52,* 5625-5628
8.	$[Zn_5(\mu_3−OH)_2(DBTA)_2(H_2O)_4]\cdot$ solvents	1591	12 wt% 2.72 mmol/g	7.1 wt% 1.61 mmol/g	*Inorg. Chem.* **2019**, *58*, 15637−15643
9.	JLU-Liu31	1700	6.86 wt% 1.56 mmol/g	3.39 wt% 0.75 mmol/g	*J. Mater. Chem. A.* **2016**, *4*, 15081-15087
10.	UCY-1	2067	6.16 wt% 1.4 mmol/g	4.31 wt% 0.98 mmol/g	*Inorg. Chem.* **2011**, *50*, 11297-11299
11.	SNU-70	5290	6.14 wt% 1.39 mmol/g	3.49 wt% 0.79 mmol/g	*Chem.− Eur. J.* **2012**, *18*, 8673 − 8680
12.	SNU-71	1770	7.75 wt% 1.76 mmol/g	4.6 wt% 1.04 mmol/g	*Chem.- Eur. J.* **2012**, *18*, 8673 − 8680
13.	Ni-MOF-1	152	7.37 wt% 1.68 mmol/g	–	*Inorg. Chem. Commun.* **2019,** *104*,78-82
14.	SALI-DAP	1225	10.1 wt%	–	*Chem. Commun.,*

Sl. No.	MOF				Reference
			2.29 mmol/g		*2015*, *51*, 12478-12481
15.	BIF-9-Li	1523	6.6 wt% 1.5 mmol/g	–	*J. Am. Chem.Soc.* **2009**, *131*, 6111-6113
16	rht-MOF-1	2100	17.7 wt% 4.02 mmol/g	10.7 wt% 2.43 mmol/g	*Chem. Commun.* **2015**, *51*, 9636-9639
17.	CAU-1	1268	24.1 wt% 5.47 mmol/g	–	*Energy Environ. Sci.* **2011**, *4*, 4522-4527
18.	{[Zn$_2$ (TPOM)(3,7-DBTDC)$_2$] ·7H$_2$O·DMA}$_n$ & {[Cd$_2$(TPOM)(3,7-DBTDC)$_2$] ·6H$_2$O·3DMF}$_n$	267 & 432	5.53 wt% 1.25 mmol/g & 7.42 wt% 1.68 mmol/g	3.69 wt% 0.83 mmol/g & 4.43 wt% 1.008 mmol/g	*ACS Appl. Mater. Interfaces* **2020**, *12*, 11724–11736
19.	FJU-44	629.5	16.38 wt% 3.72 mmol/g	–	*Inorg. Chem.* **2019**, *58*, 7754–7759
20.	**CSMCRI-9**	–	14.69 wt% 3.34 mmol/g	7.59 wt% 1.72 mmol/g	**This work**

Table S4. A comparison of catalytic performance of activated **CSMCRI-9** in CO$_2$ cycloaddition to that of other MOF materials

Sl. No.	MOF	Reaction Condition	Yield (%)	Reference
1.	Co-MOF-74	100 °C, 19.7 bar, 4 h	96	*Catal. Today* **2012**, *185*, 35-40
2.	Mg-MOF-74	100 °C, 19.7 bar, 4 h	95	*Energy Environ. Sci.* **2012,** *5*, 6465-6473
3.	Cr-MIL-101	25 °C, 8 bar, 48 h	95	*J. Catal.* **2013**, *298*, 179-185
4.	Hf-NU-1000	RT, 1 bar, 56 h	100	*J. Am. Chem. Soc.* **2014,** *136*, 15861-15864
5.	gea–MOF–1	120 °C, 20 bar, 6h	85	*Nat. Chem,* **2014**, *6*, 673–680
6.	{Cu(Hip)$_2$(Bpy)}$_n$ (CHB)	120 °C, 12bar, 6h	56	*Green Chem,* **2014**, *16*, 1607–1616
7.	Ni-TCPE2	100 °C, 9.9 bar, 12 h	86.2	*J. Am. Chem. Soc.* **2015,** *137*, 15066-

				15069
8.	Zn-NTTA	100 °C, 10bar, 8h	98.2	*ACS Appl. Mater. Interfaces* **2016**, *8*, 31746−31756
9.	UiO−67−IL	90 °C, 1 bar, 12 h	98	*Inorg. Chem,* **2017**, *56,* 2337−2344
10.	ZnMOF-1- NH$_2$	80 °C, 8bar, 8h	88	*Dalton Trans.,* **2018**, *47,* 8041−8051
11.	{[LnL(H$_2$O)$_2$]·H$_2$O}$_n$	70 °C, 1bar, 12h	89.7	*Cryst. Growth Des.* **2018**, *18,* 2956−2963
12.	MOF-892	80 °C, 1 bar, 16h	82	*ACS Appl. Mater. Interfaces* **2018**, *10,* 733−744
13.	NH$_2$−MIL−101(Al)	120 °C, 18 bar, 6h	96	*Dalton Trans.* **2018**,*47*, 418-428
14.	InDCPN-Cl	80 °C, 1 bar, 24 h	71	*Chem. Mater.* **2019**, *31,* 1084−1091
15.	[{Co(TCPB)$_{0.5}$(H$_2$O)}· DMF]$_n$	RT, 1bar, 24 h	94	*Cryst. Growth Des.* **2019**, *19,* 2010-2018
16.	{[Co(**OBA**)(L)]xG}$_n$	60 °C, 1 bar, 12 h	99	*J. Mater. Chem. A,* **2019**, *7,* 2884-2894
17.	{[Zn$_2$(3-tpom)(L)$_2$]·2H$_2$O}$_n$	40 °C, 1 bar, 24h	55	*Inorg. Chem.* **2020**, *59,* 4273−4281
18.	{[Cu-(MTABA)(H$_2$O)]·4H$_2$O ·2EtOH·DMF}$_n$	RT, 1 bar, 24 h	68	*ACS Appl. Mater. Interfaces* **2020**, *12,* 37137−37146
19.	CoMOF-2	40 °C, 1 bar, 12 h	99	*Appl. Cat. A,* **2020**, *590,* 117375
20.	**CSMCRI-9**	65°C, 10 bar, 6 h	99.9	**This work**

Table S5. Calculation of standard deviation of fluorescence intensity and limit of detection for **9a** towards DCNA

Blank Readings (9a)	Fluorescence Intensity(CPS)
Reading 1	15377871
Reading 2	15354689
Reading 3	15321964
Reading 4	15288782
Reading 5	15227191
Standard Deviation (σ)	59097.84
Slope from Graph (m)	1.858 x 10^6 μM^{-1}
Detection limit ($3\sigma/m$)	95 nM

Limit of Detection (LOD)	62.4 ppb

Table S6. Calculation of standard deviation of fluorescence intensity and limit of detection for **9a** towards TNP

Blank Readings (9a)	Fluorescence Intensity(CPS)
Reading 1	15377871
Reading 2	15354689
Reading 3	15321964
Reading 4	15288782
Reading 5	15227191
Standard Deviation (σ)	59097.84
Slope from Graph (m)	$2.679 \times 10^6 \ \mu M^{-1}$
Detection limit ($3\sigma/m$)	66 nM
Limit of Detection (LOD)	43.4 ppb

Table S7. Calculation of standard deviation of fluorescence intensity and limit of detection for **9a** towards NZF

Blank Readings (9a)	Fluorescence Intensity(CPS)
Reading 1	15377871
Reading 2	15354689
Reading 3	15321964
Reading 4	15288782
Reading 5	15227191
Standard Deviation (σ)	59097.84
Slope from Graph (m)	$956324.05 \ \mu M^{-1}$
Detection limit ($3\sigma/m$)	$0.18 \ \mu M$
Limit of Detection (LOD)	118.3 ppb

Detailed calculations of limit of detection (LOD) for 9a.

Limit of detection (LOD) = $3\sigma/k$, where σ is the standard deviation of five consecutive blank measurements of emission intensity of **9a** at regular time intervals, k = slope of the curve of decrease in fluorescence intensity of **9a** versus volume of added analyte.

Now, the five consecutive emission intensities (in CPS unit) at regular time intervals are

15377871, 15354689, 15321964, 15288782 and 15227191

Standard deviation (σ) = square root of $\{\Sigma(x_i-\mu)^2/(N-1)\}$, where x_i are the each value of emission intensity, μ is the mean of emission intensities and N is the number of intensity values.

Table S8. Calculation of standard deviation of emission intensities for **9a**

x_i	μ	$x_i-\mu$	$(x_i-\mu)^2$	$\Sigma(x_i-\mu)^2$
15377871	15314099.4	63771.6	4066816966.56	1.397×10^{10}
15354689		40589.6	1647515628.16	
15321964		7864.6	61851933.16	
15288782		-25317.4	640940742.76	
15227191		-86908.4	7553069990.56	

Here N = 5

So, σ = square root of $\{(1.397\times10^{10})/(5-1)\}$ = 59097.84

For DCNA, slope of the graph from the linear region of fluorescence intensity of **9a** versus concentration of DCNA (k) = 1.858 x 10^6 μM^{-1}

So, the LOD value for DCNA = (3×59097.84)/ 1.858×$10^6\mu M$ = 95421.7×$10^{-6}\mu M$ = 95×10^3×10^{-6}×$10^{-6}M$ = 95×10^{-9} M = 95 nM

i.e. LOD = 95 nM×mass of asymmetric unit of **CSMCRI-9** = 95×658.61 ppb = 62.4 ppb

Similarly, for TNP, slope of the graph from the linear region of fluorescence intensity of **9a**versus concentration of TNP (k) =2.679×10^6 μM^{-1}

So, the LOD value for TNP = (3×59097.84)/2.679×$10^6\mu M$ = 66178.9×$10^{-6}\mu M$ = 66×10^3× 10^{-6}×$10^{-6}M$ = 66×10^{-9} M = 66 nM

i.e. LOD = 66 nM× mass of asymmetric unit of **CSMCRI-9** = 66×658.61 ppb = 43.4 ppb

For NZF, slope of the graph from the linear region of fluorescence intensity of **9a**versus concentration of NZF (k) =956324.05 μM^{-1}

So, the LOD value for NZF = (3×59097.84)/956324.05μM = 0.18 μM.

i.e. LOD = 0.18 μM × mass of asymmetric unit of **CSMCRI-9** = 0.18×658.61 ppb = 118.3 ppb.

Table S9. A comparison of quenching constant, their LOD values, of various luminescent MOFs used for detection of DCNA

Sl. No.	LMOF/ Coordination Polymer	Quenching constant (M^{-1})	Limit of Detection (LOD)	Medium used	Ref.
1.	$\{Zn_4(TPOM)(1,4\text{-}NDC)_4\}_n$	2.74×10^4	0.28 ppm	water	*ACS Appl. Mater. Interfaces* **2018**, *10*, 42406–42416
2.	$[Zn_2(bpdc)_2(BPyTPE)]$	–	0.13 ppm	DCM	*Chem. Commun.* **2017**, *53*, 9975--9978
3.	$[Zn_2(L)_2(TPA)]. \, 2H_2O$	2.36×10^4	0.39 ppm	Methanol	*New J. Chem.* **2019**, *43*, 2353--2361
4.	$[Zn_3(DDB)(DPE)]\cdot H_2O$	3.3×10^4	166 ppb	water	*Dalton Trans.*, **2019**, *48*, 16776–16785
5.	$[Cd_3(CBCD)_2(DMA)_4(H_2O)_2]\cdot 10DMA$	4.47×10^4	145 ppb	DMA	*Dalton Trans.* **2019**, *48*, 2683–2691
6.	$[Mg_2(APDA)_2(H_2O)_3]\cdot 5DMA\cdot 5H_2O$	7.50×10^4	150 ppb	DMF	*Inorg. Chem.* **2018**, *57*, 13330–13340
7.	$[Ag(CIP^-)]$	5.2×10^4	105 ppb	DMF	*Dalton Trans.* **2019**, *48*, 10892–10900
8.	**CSMCRI-9**	4.96×10^4	95 nM 62.4 ppb	water	**This work**

Table S10. A comparison of quenching constant, their LOD values, of various luminescent MOFs used for detection of TNP

Sl. No.	LMOF/Coordination polymer	Quenching constant (M^{-1})	Limit of Detection (LOD)	Medium used	Ref.
1.	bio- MOF-1 $[Zn_8(ad)_4(BPDC)_6O\cdot 2\,Me_2NH_2]\cdot G$ (G=DMF and water)	4.6×10^4	12.9 nM (2.9 ppb)	water	*Chem. –Eur. J.*, **2015**, *21*, 965 – 969
2.	Ur-MOF $[Zn_4(DMF)\,(Ur)_2(NDC)_4]$	10.83×10^4	7.1 µM (1.63 ppm)	water	*Cryst. Growth Des.*, **2015**, *15*, 4627–4634
3.	$Zn_2(H_2L)_2(Bpy)_2(H_2O)_3\cdot H_2O$	1.36×10^4	0.49 µM	water	*Cryst. Growth Des.* **2017**, *17*, 3170-3177
4.	$\{[Cd_2(tdz)_2(4,4'\text{-}bpy)_2]\cdot 6.5H_2O\}_n$	4.86×10^4	1.4 ppm	water	*Dalton Trans.*, **2019**, *48*, 2388-2398
5.	$[Tb_2(L_9)_3(H_2O)_2].21H_2O$	9.2×10^3	67 ppb	water	*J. Mater. Chem. A*, **2017**, *5*, 1952-

					1956
6.	$[Cd(L_4)(L_5)]_n$	2.68×10^4	0.27 µM (62 ppb)	water	*Dalton Trans.*, **2016**, *45*, 7881-7892
7.	$\{[Zn_2(TPOM)(NH_2\text{-}BDC)_2].4H_2O\}_n$	4.6×10^4	0.98 µM	DMF	*J. Mater. Chem. A*, **2016**, *4*, 15494–15500
8.	BUT-12 $[Zr_6O_4(OH)_8(H_2O)_4(CTTA)_{8/3}]$	3.1×10^5	23 ppb	water	*J. Am. Chem. Soc.*, **2016**, *138*, 6204–6216
9.	$\{[Cd_4(L_6)_2(2\text{-amino-4,4-bipyridine})_3(H_2O)_2](8DMF)(8H_2O)\}_n$	3.89×10^4	1.98 ppm	Ethanol	*Inorg. Chem.* **2016**, *55*, 1741-1747
10.	$[(CH_3)_2NH_2]_3[Zn_4Na(L_3)_3].4CH_3OH.2DMF$	3.2×10^4	5 µM	DMF	*J. Mater Chem. A* **2015**, 3, 7224-7228
11.	$\{[W_2(\mu_3\text{-}S)_6(\mu_4\text{-}S)_2Cu_8(CN)_4(3\text{-abpt})]\cdot CH_3CN\cdot H_2O\}_n$	7.66×10^4	0.81 µM	Acetonitrile	*Inorg. Chem.* **2019**, *58*, 9749-9755
12.	$[Tb(TCBA)(H_2O)_2]_2\cdot DMF$	4.69×10^6	1.64 ppb	Ethanol	*Inorg. Chem.* **2019**, *58*, 8198-8207
13.	$\{[Cd(ATAIA)].4H_2O\}_n$	1.59×10^7	0.94 nM	Water	*ACS Appl. Mater. Interfaces* **2018**, *10*, 25360–25371
14.	$[Tb(1,3,5\text{-BTC})]_n$	3.4×10^4	81 nM	Ethanol	*J. Mater. Chem. A*, **2013**, *1*, 8745–8752
15.	**CSMCRI-9**	2.46×10^4	66 nM 43.4 ppb	water	**This work**

Table S11. A comparison of quenching constant, their LOD values, of various luminescent MOFs used for detection of NZF

Sl. No.	LMOF/ Coordination Polymer	Quenching constant (M^{-1})	Limit of Detection (LOD)	Medium used	Ref.
1.	$[Mg_2(APDA)_2(H_2O)_3].5DMA.5H_2O$	9.00×10^4	108 ppb	DMF	*Inorg. Chem.* **2018**, *57*, 13330–13340
2.	$[Cd_3(CBCD)_2(DMA)_4(H_2O)_2]\cdot 10DMA$	9.72×10^4	85 ppb	DMA	*Dalton Trans.* **2019**, *48*, 2683–2691
3.	BUT-12 BUT-13	1.1×10^5 7.5×10^4	58 ppb 90 ppb	water	*J. Am. Chem. Soc.* **2016**, *138*, 6204–6216

4.	{[Eu$_2$(BCA)$_3$(H$_2$O)(DMF)$_3$]·0.5DMF·H$_2$O}$_n$	2.2×10^4	0.16 µM	water	Chem.−Eur. J. 2017, 23, 10293 – 10300
5.	{[Zn$_2$(Py$_2$TTz)$_2$(BDC)$_2$]·2(DMF)·0.5(H$_2$O)}$_n$	1.726×10^4	0.91 µM	water	Cryst. Growth Des. 2018, 18, 7173−7182
6.	TMPyPE@bio-MOF-1	4.48×10^4	0.11 ppm	water	J. Mater. Chem. C, 2019, 7, 8383--8388
7.	{[Tb(TATMA)(H$_2$O)·2H$_2$O}$_n$	3.0×10^4	NA	water	Inorg. Chem. 2019, 58, 7746−7753
8.	[(Zn$_4$O)$_2$(PDDA)$_6$(H$_2$O)$_2$]·10DMF	6.08×10^4	NA	DMF	Cryst. Growth Des. 2019, 19, 5228−5236
9.	[NaCd$_2$(L)(BDC)$_{2.5}$].9H$_2$O	5.06×10^4	162 ppb	DMF	J. Mater. Chem. A, 2017, 5, 15797−15807
10.	**CSMCRI-9**	4.81×10^4	0.18 µM 118.3 ppb	water	**This work**

Table S12. HOMO and LUMO energy levels of different pesticides calculated by density functional theory (DFT) at B3LYP/6-311++G** accuracy level, using Gaussian 09 package of programs

Analytes	HOMO (eV)	LUMO (eV)	Energy gap (eV)
DCNA	-6.67	-3.01	3.66
TCHDE	-6.47	-1.33	5.14
DCP	-6.64	-1.15	5.49
HCL	-7.12	-1.17	5.95
IPT	-6.04	-0.56	5.48
BHP	-6.08	-0.70	5.38
DUN	-6.34	-1.06	5.28
bpg	-7.47	-1.55	5.92

Table S13. HOMO and LUMO energy levels of different nitroanalytes calculated by density functional theory (DFT) at B3LYP/6-311++G** accuracy level, using Gaussian 09 package of programs

Analytes	HOMO (eV)	LUMO (eV)	Energy gap (eV)
TNP	-8.61	-4.30	4.31
2,4-DNP	-8.05	-3.77	4.28
4-NP	-7.34	-2.75	4.59
3-NP	-7.20	-2.90	4.30
2-NP	-7.22	-3.18	4.04
2,4-DNT	-8.42	-3.39	5.03
4-NT	-7.70	-2.79	4.91
DMDNB	-8.65	-2.83	5.82
bpg	-7.47	-1.55	5.92

Table S14. HOMO and LUMO energy levels of different antibiotics calculated by density functional theory (DFT) at B3LYP/6-311++G** accuracy level, using Gaussian 09 package of programs

Analytes	HOMO (eV)	LUMO (eV)	Energy gap (eV)
NZF	-6.79	-3.14	3.65
NFT	-7.37	-3.66	3.71
FZD	-7.15	-3.49	3.66
DTZ	-7.30	-2.76	4.54
MDZ	-7.34	-2.85	4.49
ODZ	-7.32	-2.89	4.43
SMZ	-6.53	-1.17	5.36
SDZ	-6.59	-1.46	5.13
THI	-7.70	-2.00	5.70
bpg	-7.47	-1.55	5.92

References

1. *SAINT+*, version 6.02; Bruker AXS: Madison, WI, 1999.

2. G. M. Sheldrick, *SADABS*, Empirical Absorption Correction Program; University of Göttingen: Göttingen, Germany, 1997.

3. *XPREP*, version 5.1; Siemens Industrial Automation Inc.: Madison, WI, 1995.

4. G. M. Sheldrick, *SHELXTL* Reference Manual: version 5.1; Bruker AXS: Madison, WI, 1997.

5. G. M. Sheldrick, *SHELXL-2014/7*; University of Göttingen: Göttingen, Germany.

6. A. L. Spek, *PLATON*; The University of Utrecht: Utrecht, The Netherlands, 1999.

7. http://www.topos.ssu.samara.ru; V. A. Blatov, IUCrCompCommNewsletter 2006, 7, 4.

8. S. Nandi, D. Chakraborty, R. Vaidhyanathan, Permanently Porous Single Molecule H-Bonded Organic Framework for Selective CO_2 Capture, *Chem. Commun*. 2016, **52**, 7249-7252.

9. Y. Yuan, J. T. Li, X. D. Sun, G. H. Li, Y. L. Liu, G. Verma and S. Q. Ma, Indium–organic frameworks based on dual secondary building units featuring halogen-decorated channels for highly effective CO_2 fixation, *Chem. Mater*., 2019, **31**, 1084–1091.